

# VLT-VIMOS integral field spectroscopy of luminous and ultraluminous infrared galaxies

## II. Evidence for shock ionization caused by tidal forces in the extra-nuclear regions of interacting and merging LIRGs<sup>★</sup>

Ana Monreal-Ibero<sup>1</sup>, Santiago Arribas<sup>2</sup>, Luis Colina<sup>2</sup>, Javier Rodríguez-Zaurín<sup>2</sup>,  
Almudena Alonso-Herrero<sup>2</sup>, and Macarena García-Marín<sup>3</sup>

<sup>1</sup> European Organisation for Astronomical Research in the Southern Hemisphere (ESO); Karl-Schwarzschild-Strasse 2 D-85748 Garching bei München

e-mail: amonreal@eso.org

<sup>2</sup> Departamento de Astrofísica Molecular e Infrarroja (DAMIR), Instituto de Estructura de la Materia (IEM/CSIC); c/ Serrano 121, 28996 Madrid

e-mail: [arribas,colina,aalonso,jrz]@damir.csic.es

<sup>3</sup> I. Physikalisches Institut, Universität zu Köln Zùlpicher Strasse 77, 50937 Köln, Germany

e-mail: maca@ph1.uni-koeln.de

accepted version

### ABSTRACT

**Context.** Luminous infrared galaxies (LIRGs) are an important class of objects in the low- $z$  universe bridging the gap between normal spirals and the strongly interacting and starbursting ultraluminous infrared galaxies (ULIRGs). Since a large fraction of the stars in the Universe have been formed in these objects, LIRGs are also relevant in a high- $z$  context. Studies of the two-dimensional physical properties of LIRGs are still lacking.

**Aims.** We aim to understand the nature and origin of the ionization mechanisms operating in the extra-nuclear regions of LIRGs as a function of the interaction phase and infrared luminosity.

**Methods.** This study uses optical integral field spectroscopy (IFS) data obtained with VIMOS. Our analysis is based on over 25 300 spectra of 32 LIRGs covering all types of morphologies (isolated galaxies, interacting pairs, and advanced mergers), and the entire  $10^{11} - 10^{12} L_{\odot}$  infrared luminosity range.

**Results.** We found strong evidence for shock ionization, with a clear trend with the dynamical status of the system. Specifically, we quantified the variation with interaction phase of several line ratios indicative of the excitation degree. While the  $[\text{N II}]\lambda 6584/\text{H}\alpha$  ratio does not show any significant change, the  $[\text{S II}]\lambda 6717, 6731/\text{H}\alpha$  and  $[\text{O I}]\lambda 6300/\text{H}\alpha$  ratios are higher for more advanced interaction stages. Velocity dispersions are higher than in normal spirals and increase with the interaction class (medians of 37, 46, and 51  $\text{km s}^{-1}$  for class 0, 1, and 2, respectively). We constrained the main mechanisms causing the ionization in the extra-nuclear regions (typically for distances ranging from  $\sim 0.2$ - $2.1$  kpc to  $\sim 0.9$ - $13.2$  kpc) using diagnostic diagrams. Isolated systems are mainly consistent with ionization caused by young stars. Large fractions of the extra-nuclear regions in interacting pairs and more advanced mergers are consistent with ionization caused by shocks of  $v_s \lesssim 200 \text{ km s}^{-1}$ . This is supported by the relation between the excitation degree and the velocity dispersion of the ionized gas, which we interpret as evidence for shock ionization in interacting galaxies and advanced mergers but not in isolated galaxies. This relation does not show any dependence with the infrared luminosity (i.e. the level of star formation). All this indicates that tidal forces play a key role in the origin of the ionizing shocks in the extra-nuclear regions. We also showed for the first time what appears to be a common  $\log([\text{O I}]\lambda 6300/\text{H}\alpha) - \log(\sigma)$  relation for the extranuclear ionized gas in interacting (U)LIRGs (i.e. covering the entire  $10^{11.0} - 10^{12.3} L_{\odot}$  luminosity range). This preliminary result needs to be investigated further with a larger sample of ULIRGs.

**Key words.** Galaxies: active — Galaxies: interactions — Galaxies: starburst — Infrared: galaxies

### 1. Introduction

Luminous and ultraluminous infrared galaxies (LIRGs and ULIRGs) are defined as those objects with an infrared luminosity of  $L_{\text{IR}} = L(8 - 1000 \mu\text{m}) = 10^{11} - 10^{12} L_{\odot}$  and  $L_{\text{IR}} \gtrsim 10^{12} L_{\odot}$ , respectively (see Sanders & Mirabel 1996; Lonsdale et al. 2006, for a review). They are systems which contain large amounts

of gas and dust (e.g. Evans et al. 2002) and which are undergoing an intense star-formation episode in their (circum)nuclear regions (e.g. Scoville et al. 2000; Alonso-Herrero et al. 2006). This activity is the main cause of their huge luminosity in about  $\sim 80\%$  of these systems, although some contribution from an AGN is present and even dominant in some cases (e.g. Genzel et al. 1998; Risaliti et al. 2006; Farrah et al. 2007; Nardini et al. 2008).

These systems usually present some degree of interaction whose importance increases with luminosity. While the majority of local LIRGs can be classified as isolated spirals or interact-

Send offprint requests to: A. Monreal-Ibero

<sup>★</sup> Based on observations collected at the European Organisation for Astronomical Research in the Southern Hemisphere, Chile (ESO Programs 076.B-0479(A), 078.B-0072(A) and 081.B-0108(A)).

ing pairs (e.g. Arribas et al. 2004; Alonso-Herrero et al. 2006; Sanders & Ishida 2004), most of the ULIRGs show signs of a clear merging process (e.g. Clements et al. 1996; Borne et al. 2000; Cui et al. 2001; Bushouse et al. 2002; Veilleux et al. 2002). While (U)LIRGs are an oddity in the local Universe, recent mid-infrared and submillimeter surveys show how they present a strong evolution with redshift, increasing their number by two orders of magnitude at  $z \sim 0.8 - 1.2$  (Elbaz et al. 2002). Indeed they are the dominant population of the infrared selected galaxies at high redshift, making a significant contribution to the star-formation rate density at  $0.5 < z < 2$  (Pérez-González et al. 2005; Le Flocc’h et al. 2005).

The study of the ionization properties of the gas in these objects is relevant for two main reasons. On the one hand, the ionization is important to investigate the nature (i.e. starburst, AGN) of the dominant source that causes the huge luminosity in the infrared. In the optical, this has mainly been done via long-slit observations of the nuclear regions of large samples of (U)LIRGs (e.g. Kim et al. 1995; Veilleux et al. 1999, and references therein). These studies established trends with the luminosity and interaction stage, and found an increase in the frequency of AGN-dominated systems with luminosity. These results have been recently revisited using the new optical classifications provided by the use of *Sloan Digital Sky Survey* (SDSS) data (Yuan et al. 2010). They show that most of the (U)LIRGs previously classified as *Low-ionization nuclear emission-line region* (LINER), now are classified as starburst-AGN composite galaxies. The presence of an obscured AGN has been also revealed by the detection of ionization cones with integral field spectroscopy (IFS) data (e.g. Arp 299, García-Marín et al. 2006).

On the other hand, the ionization structure helps to understand how the interaction/merger process as well as the release of energy and material from the central source and/or starbursts are affecting the extended structure of the galaxies in general and its interstellar medium in particular. In that sense, the presence of Super Galactic Winds (SGWs) in (U)LIRGs has been suggested using emission (Heckman et al. 1990; Lehnert & Heckman 1996) and absorption (Heckman et al. 2000; Rupke et al. 2002, 2005a,b) lines. Tidally induced forces associated with the interaction process itself have been also suggested as the cause for the ionization of the gas (McDowell et al. 2003; Colina et al. 2005). Given the complex structure of these systems, where the selection of a preferential direction is specially difficult, these studies would benefit from IFS data thanks to which it is possible to obtain homogeneous two-dimensional spectral information.

Using this technique Monreal-Ibero et al. (2006, hereafter MAC06) have studied a sample of six ULIRGs (nine galaxies), and found that wide areas of the extra-nuclear extended regions presented line ratios typical of LINERs according to the diagnostic diagrams of Veilleux & Osterbrock (1987). In addition, it was shown that the velocity dispersion is positively correlated with the degree of ionization supporting the idea that shocks are the main cause of the ionization in these areas. However, these results were based on a relatively small sample, which covered a restricted range in luminosity ( $\log(L_{IR}/L_{\odot}) = 12.03 - 12.40$ ) and interaction phase.

In this paper we extend that study to a larger sample of 32 systems, which cover the entire  $\log(L_{IR}/L_{\odot}) = 11.00 - 12.00$  luminosity range (i.e. the LIRGs range), and the different interaction types (i.e., isolated galaxies, interaction pairs, and mergers remnants).

The present study is part of a wider project devoted to the study of the internal structure and kinematics of a represen-

tative sample of low-redshift LIRGs and ULIRGs using optical and near-IR IFS facilities (Arribas et al. 2008). Specifically we used the INTEGRAL+WYFFOS facility (Arribas et al. 1998; Bingham et al. 1994) and the *Potsdam Multi-Aperture Spectrograph*, PMAS (Roth et al. 2005) in the Northern Hemisphere, and VIMOS (LeFèvre et al. 2003) and SINFONI (Eisenhauer et al. 2003) in the southern one. The corresponding catalogs for the PMAS, INTEGRAL and VIMOS samples can be found in Alonso-Herrero et al. (2009), García-Marín et al. (2009) and Rodríguez-Zaurín et al. (in prep.), respectively.

The paper is structured as follows: in Sect. 2 we describe the sample used in this work as well as the characteristics of the instrumental configuration and technical details regarding data reduction and analysis; Sect. 3 quantifies how the ionization degree varies with interaction stage and constrains the possible mechanisms that cause the ionization of the gas. Finally, a comparison with the previous results for ULIRGs and a discussion about the origin of the ionization produced by shocks in terms of the star formation and the interaction process are presented.

Throughout the paper, a cosmology with  $70 \text{ km s}^{-1} \text{ Mpc}^{-1}$ ,  $\Omega_M = 0.3$  and  $\Omega_{\Lambda} = 0.7$  is assumed.

## 2. The data

### 2.1. The sample

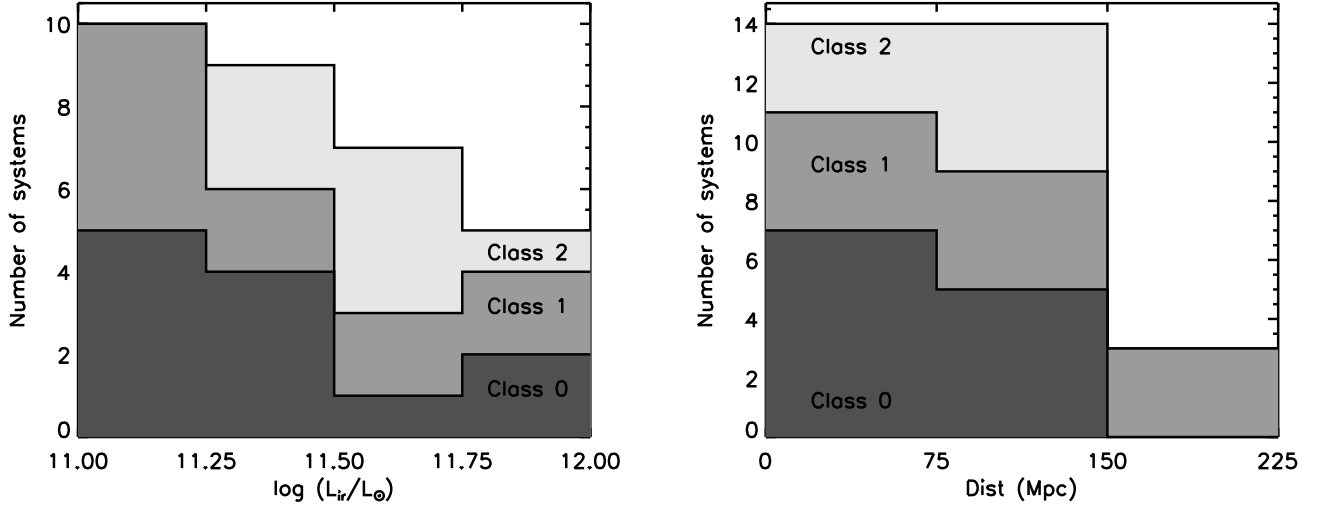
The present sample is drawn from the VIMOS IFS sample of (U)LIRGs presented in Arribas et al. (2008, hereafter, Paper I). Specifically, it includes all the LIRGs listed in that paper, except for IRAS F10173+0828, for which no emission lines were detected. That implies 32 systems, of which 13 were isolated, 11 interacting systems (9 pairs and 2 triple), and 8 advanced mergers (i.e. classes 0, 1, and 2, respectively, according to Paper I terminology). The methodology followed to perform the morphological classification is described below.

Figure 1 summarizes the distribution in luminosity, distance, and interaction type of the systems in our final sample. The mean distance of the sample is 87 Mpc, which leads to a mean linear scale of  $\sim 400 \text{ pc arcsec}^{-1}$ . Taking into account the VIMOS spaxel size of  $0''.67$ , this translates into a mean linear spatial sampling of the source of  $\sim 270 \text{ pc spaxel}^{-1}$ . We refer the reader to Table 1 in Paper I for the basic properties of the individual systems.

### 2.2. Morphological classification

Our morphological/merging classification is a simplified version of that proposed by Veilleux et al. (2002) for ULIRGs, who divided their sample in five classes (and four sub-classes). We only considered three main classes (i.e. "isolated": 0, "interacting": 1, "merger": 2) to reduce uncertainties associated with sorting. In particular, the different morphological classes considered are

- Class 0: Objects that appear to be single isolated galaxies, with a relatively symmetric morphology and without evidence for strong past or ongoing interaction.
- Class 1: Objects in a pre-coalescence phase with two well differentiated nuclei separated by a projected distance of  $D > 1.5 \text{ kpc}$ . For those objects classified as 1, it is still possible to identify the individual merging galaxies and their corresponding tidal structures due to the interaction. The limit of 1.5 kpc was chosen because theoretical models predict a fast coalescence phase after the nuclei become closer than that distance (e.g. Mihos & Hernquist 1996; Naab et al. 2006).



**Fig. 1.** Histograms showing the luminosity (*left*) and distance (*right*) distributions of the systems in the sample. Light, intermediate and dark gray areas indicate the total number of isolated galaxies (class 0), interacting systems (class 1), and merger remnants (class 2), respectively (see text for a more detailed definition of the different morphological types).

- Class 2: Objects with a relatively asymmetric morphology suggesting a post-coalescence merging phase. They may have two nuclei separated a projected distance of  $D \leq 1.5$  kpc. For objects classified as 2, it is not possible to identify the interacting galaxies individually.

For simplicity we will refer to objects of classes 0, 1, and 2 as “isolated”, “interacting”, and “merger” systems.

The classification was primarily based on the Digital Sky Survey (DSS) images, which are available for all the sources on the NASA Extragalactic database (NED). In most of the cases these images are sufficient to classify the objects of the present sample. However, for seven objects (less than 25% of the sample), the DSS images were not conclusive. In these cases (IRAS 08355–4944, IRAS F08520–6850, IRAS F10038–3338, IRAS F12116–5610, IRAS F13001–2339, IRAS F17138–1017 and IRAS F21453–3511) high-resolution HST images were used as supplementary information, mainly from program ID:10582 (IP: Evans). For another six objects the HST images just confirm the morphological classification derived using the DSS images. In Figure 14 (on-line) we present the images used for the classification. In some cases the dynamic range is large and the different relevant features appear at quite different intensity levels, so we recommend the reader interested in a particular case to directly download and display the images.

In order to estimate the uncertainty associated with this classification process, we thrice classified the whole sample independently. The level of agreement was higher than 90%. However, there were intrinsically difficult cases for which we agreed they have an uncertain classification. These cases are: IRAS 09437+0317 (IC 563/IC 564) (1/0), IRAS F12116–5615 (2/0), IRAS F13001–2339 (2/1), and IRAS F17138–1017 (2/0), and they will not be considered later when analyzing the global behavior of the different classes.

Further details on the morphology of these objects may be found in Rodríguez-Zaurín et al. (in prep.).

### 2.3. Observations and instrumental set-up

A detailed description of the observations is provided in Paper I. Here we briefly recall the observational set-up and characteristics of the data.

The data were obtained in service mode with the VIMOS-IFU at VLT during semesters 76, 78, and 81. We used the HR-Orange configuration, which covers the 5250 – 7400 Å spectral range with a resolution of 3400. It provides a field-of-view of  $27'' \times 27''$  with  $0''.67$  per spatial element (*spaxel*) making a total of 1600 spectra per pointing. Each galaxy was observed using a 4-pointing dither pattern with a relative off-set of  $2''.7$  (i.e. four spaxels) to minimize the effect of dead fibers and thus, providing an effective field-of-view of about  $29''.7 \times 29''.7$ . Details about data reduction and line fitting can be found in Paper I.

### 2.4. Emission line data

We used in our analysis the  $[\text{O I}]\lambda 6300$ ,  $\text{H}\alpha$ ,  $[\text{N II}]\lambda 6548, 6584$ , and  $[\text{S II}]\lambda 6717, 6730$  emission lines, which were fitted to a single Gaussian component. For some galaxies, small areas of the  $\text{H}\alpha$  emission showed evidence for two or more kinematically distinct components. These particular areas of double components are generally associated with nuclear regions (i.e. IRAS F08520–6850, IRAS F13229–2934, the eastern member of IRAS F14544–4255 and IRAS 21453–3511) which are not used in the present analysis (see below). In some cases these also affect small areas in the extranuclear regions (IRAS F06592–6313, IRAS F07160–6215, IRAS F10409–4556, IRAS F13229–2934, IRAS 08424–3130, IC 564, the western member of IRAS F14544–4255, the northern and central members of IRAS 18093–5744, IRAS F04315–0840, IRAS 10257–4338, IRAS 17138–1017 and IRAS 21453–3511). For a given galaxy, these regions represent typically less than 5% of the data. In those cases where the two components were clearly distinguishable, the dominant component was used in the present analysis, while in those of strong blending we used the results from the one-profile fit. A more detailed analysis of the regions where multiple components

are identified is out of the scope of the present paper and will be presented with the full kinematic analysis in a future paper.

Thus a measure of the flux in the different emission lines as well as one independent measurement of the central wavelength and FWHM (full width at half maximum) is obtained for each spectrum. The FWHM has been corrected from the instrumental width measured with the strong [O I] $\lambda$ 6300 Å sky line, and then translated into velocity dispersions. For the VIMOS configuration used, the spectral resolution translates into an instrumental width  $\sigma_{ins} \sim 38 \pm 8 \text{ km s}^{-1}$ . The corresponding values for the weaker [O I] $\lambda$ 6363 Å sky line are  $\sigma_{ins} \sim 33 \pm 10 \text{ km s}^{-1}$ . Therefore, the profiles of the emission lines will be considered as resolved if their observed profile is wider than  $50 \text{ km s}^{-1}$  ( $\sigma_{obs}$ ). In general the [O I] $\lambda$ 6300, [S II] $\lambda$ \lambda6717,6731, [N II] $\lambda$ \lambda6584, and H $\alpha$  emission lines define a sequence of increasing S/N and, therefore, the [N II] $\lambda$ 6584/H $\alpha$  maps cover a larger area than those generated with the other line ratios. While uncertainties in the line flux for the strongest emission lines (H $\alpha$ ) in high surface-brightness regions are about 10%, weaker lines like [S II] $\lambda$ \lambda6717,6731 and [O I] $\lambda$ 6300 can have large uncertainties due to the lower S/N. However, no lines with flux uncertainties larger than 30% are used in the analysis presented in this paper. So, the typical uncertainties in the line ratios varies from about 15% for high S/N lines to about 30% for low surface brightness and when a weak line is involved.

Similarly to MAC06, we only used the extra-nuclear regions of our galaxies for the analysis in this paper. To do so, we excluded the nuclear regions, defined as those within the central 3 spaxel $\times$ 3 spaxel (2'0 $\times$ 2'0) where, in addition to the complex line profiles mentioned above, contamination due to a dust enshrouded AGN could affect the results. For the typical distances of our sample of LIRGs, this corresponds to a region of about  $\sim 800 \text{ pc} \times 800 \text{ pc}$  in size. For the particular case of IRAS F04315-0840, where the two galaxies are coalescing, the area with emission lines presenting double components was a bit larger than the standard 3 spaxel $\times$ 3 spaxel one. Because here the one Gaussian approach did not properly reproduce the line profiles, we made an exception and also masked the corresponding spaxels (see Fig. 2).

The final total number of available data points, mean and standard deviation for each individual pointing for the three line ratio used as well as the velocity dispersion inferred from H $\alpha$  are shown in Table 1.

### 3. Results and discussion

#### 3.1. General characteristics of the excitation maps

Figure 2 presents the [N II] $\lambda$ 6584/H $\alpha$ , [S II] $\lambda$ \lambda6717,6731/H $\alpha$ , and [O I] $\lambda$ 6300/H $\alpha$  line ratio maps for each individual VIMOS pointing. Although these maps only represent one axis of the classical BPT diagrams (Baldwin et al. 1981; Veilleux & Osterbrock 1987), they are good tracers of the excitation when studying the general properties of the extra-nuclear ionized regions of LIRGs. In fact, in the X-[O III] $\lambda$ 5007/H $\beta$  diagnostic diagrams (where X is any of the above line ratios), the boundaries distinguishing regions mainly photo-ionized by stars (i.e. H II-like) and those of LINER type are nearly vertical for the expected values of  $\log([O III]\lambda 5007/H\beta)$  in these extra-nuclear regions ( $\sim -0.2$ , see below). Figure 2 also shows the H $\alpha$  surface brightness maps. These maps are presented here mainly as a reference for the excitation maps, and they will be discussed in detail elsewhere (Rodríguez-Zaurín et al. in prep.). The different area covered by the excitation maps is a direct con-

sequence of the different signal-to-noise (S/N) of the involved lines. The [N II] $\lambda$ 6584/H $\alpha$  map encompasses the largest area in all the cases, reaching areas of low H $\alpha$  surface brightness where no good S/N data are available for the [O I] $\lambda$ 6300 and [S II] $\lambda$ \lambda6717,6731 lines.

The star-forming regions of relatively low excitation are well identified in the maps. These are generally high H $\alpha$  surface brightness regions associated with large scale structures like spiral arms (e.g. IRAS F13229–2934), rings (e.g. IRAS F11255–4120), or tidal tails (e.g. IRAS 06076–2139). However, knots of star formation are also found in isolated external regions (e.g. IRAS F12115–4656, IRAS F07027–6011 S). In some cases these external regions define a chain suggestive of star formation along tidal tails (e.g. IRAS F11506–3851, IRAS 06076–2139, Paper I).

Galaxies in double or triple systems may have quite different excitation conditions, indicating that the interstellar medium of the individual objects have different properties. For instance, while the external regions of the central and southern component of IRAS F06259–4708 are dominated by star formation, for the northern galaxy these regions show higher excitation (similarly for IRAS F06076–2139).

Interestingly the external regions associated to diffuse low surface brightness H $\alpha$  emission have relatively high excitation. In these regions the line ratios could, in principle, be affected by an underlying absorption spectrum. Indeed, preliminary results for our PMAS sample of LIRGs (Alonso-Herrero et al. 2009) show that for spectra with  $EW(H\alpha) \leq 10 \text{ \AA}$ , the line ratio can decrease  $\sim 0.2$  dex once the contribution of an old stellar population has been taken into account (Alonso-Herrero et al. 2010). In order to quantify the effect of a possible component in absorption, we created maps including a correction of  $EW_{abs} = 2 \text{ \AA}$ . [S II] $\lambda$ \lambda6717,6731/H $\alpha$  and [O I] $\lambda$ 6300/H $\alpha$  line ratios are affected by about 0.2 dex for only a handful ( $\leq 2\%$ ) of spaxels, and by less than 0.1 dex, for most of the data. For the [N II] $\lambda$ 6584/H $\alpha$  line ratio, this effect could reach  $\sim 0.3$  dex in the very low surface brightness areas, but does not change in any case the observed ionization structure that we describe here. These regions of low H $\alpha$  surface brightness and relatively high excitation are found in all kind of objects: structured systems with rings (IRAS 10567–4310) and spiral (IRAS F04315–0840) morphologies, highly disturbed systems (the central member of IRAS F07160–5744), and galaxies with relatively round/ elliptical shape (IRAS F11506–3851). In objects with round morphologies this transition from low to high excitation translates into the appearance of external rings of high excitation (IRAS F11506–3851, IRAS F12115–4656). The transition from low to high excitation is also observed in the triple system IRAS 18093–5744 where an extension (tidal tail?) from the main body of the central galaxy towards the northern galaxy is identified. In some cases the high-excitation regions are found close to the nucleus and/or along preferential directions, and defining structures suggestive of cones. Some examples are IRAS F10409–4556, ESO 297–G012 or the southern member of IRAS 12042–3140.

For the rest of the paper we will focus on the study of the extra-nuclear excitation conditions using the presented line ratios as well as the velocity dispersions.

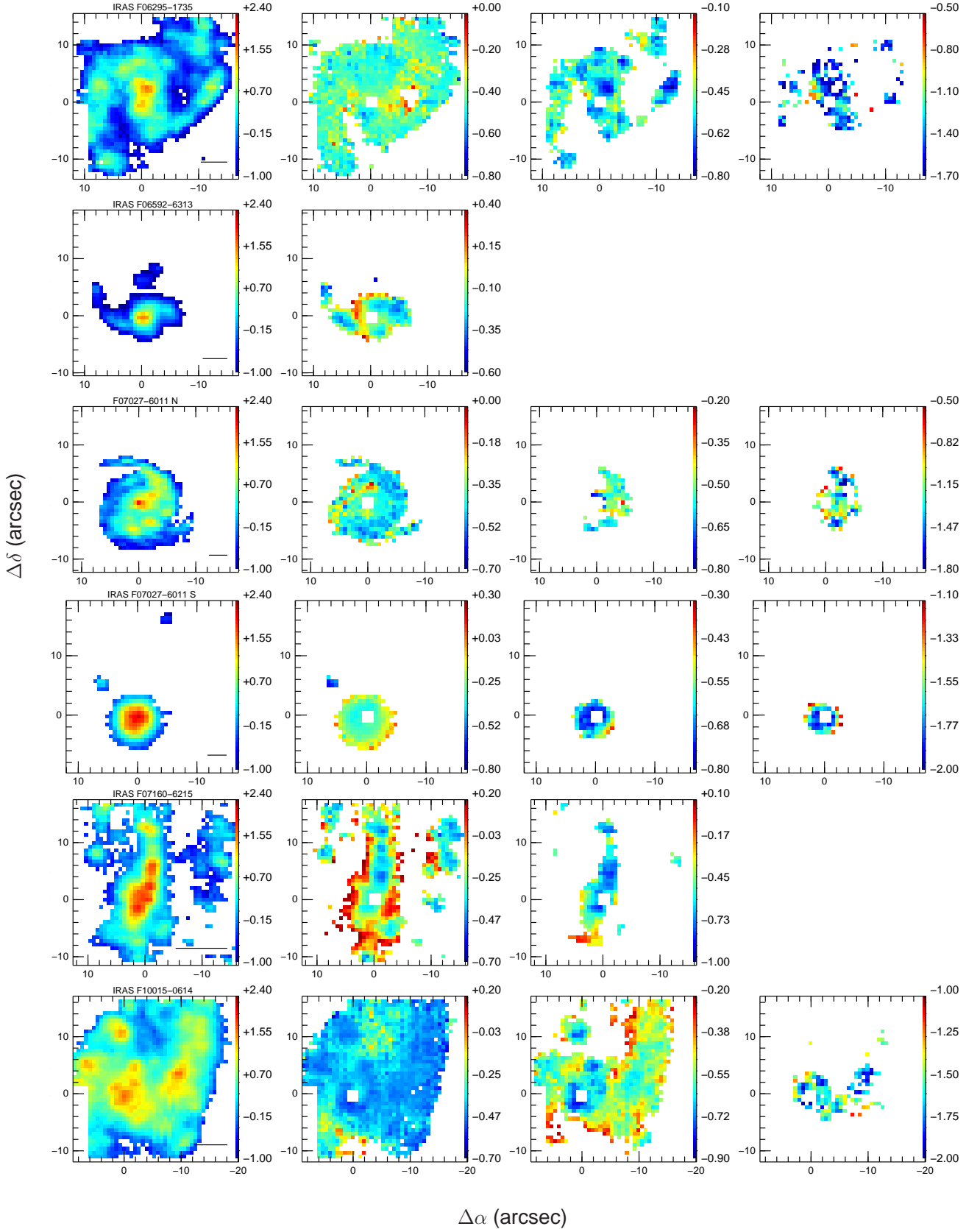


**Fig. 2.** Maps for  $H\alpha$  and  $[N\ II]\lambda 6584/H\alpha$ ,  $[S\ II]\lambda\lambda 6717,6731/H\alpha$ , and  $[O\ I]\lambda 6300/H\alpha$  line ratios for our LIRGs sample. Each row shows a VIMOS pointing. The nuclear masked areas not considered in this work are represented in the line ratio maps as white squares.  $H\alpha$  intensity is displayed in arbitrary units and using a logarithmic scale to better emphasize all the morphological features. The physical scale of 2 kpc at the distance of the galaxy is represented by the straight line in the bottom right corner. Axes scales are in arcsec and orientation is as usual: north up, east to the left.

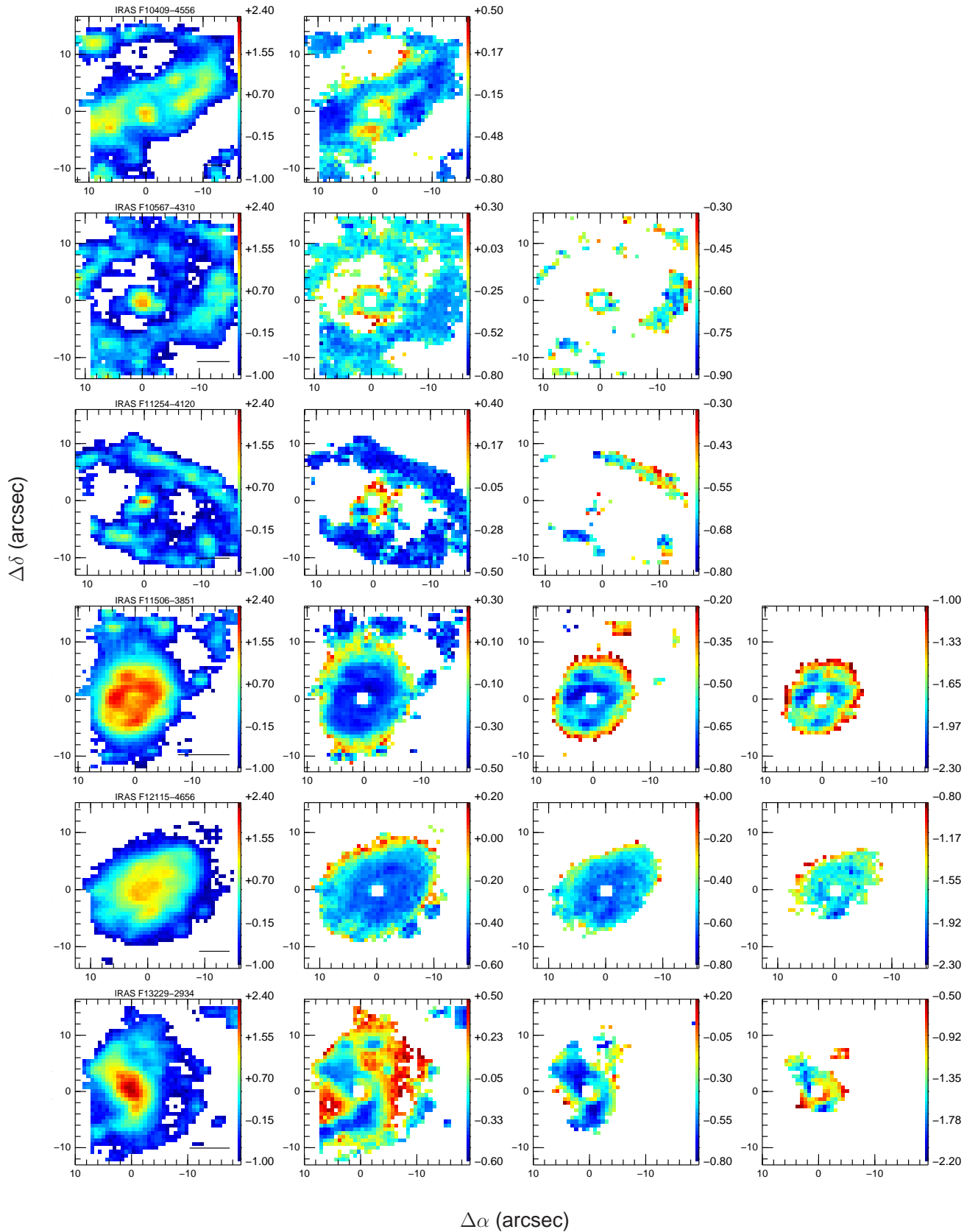


Fig. 2. continued.

### 3.2. Dependence of the excitation conditions of the extra-nuclear ionized gas with the interaction class

In order to investigate possible changes in the excitation properties of the ionized gas as a consequence of interactions and

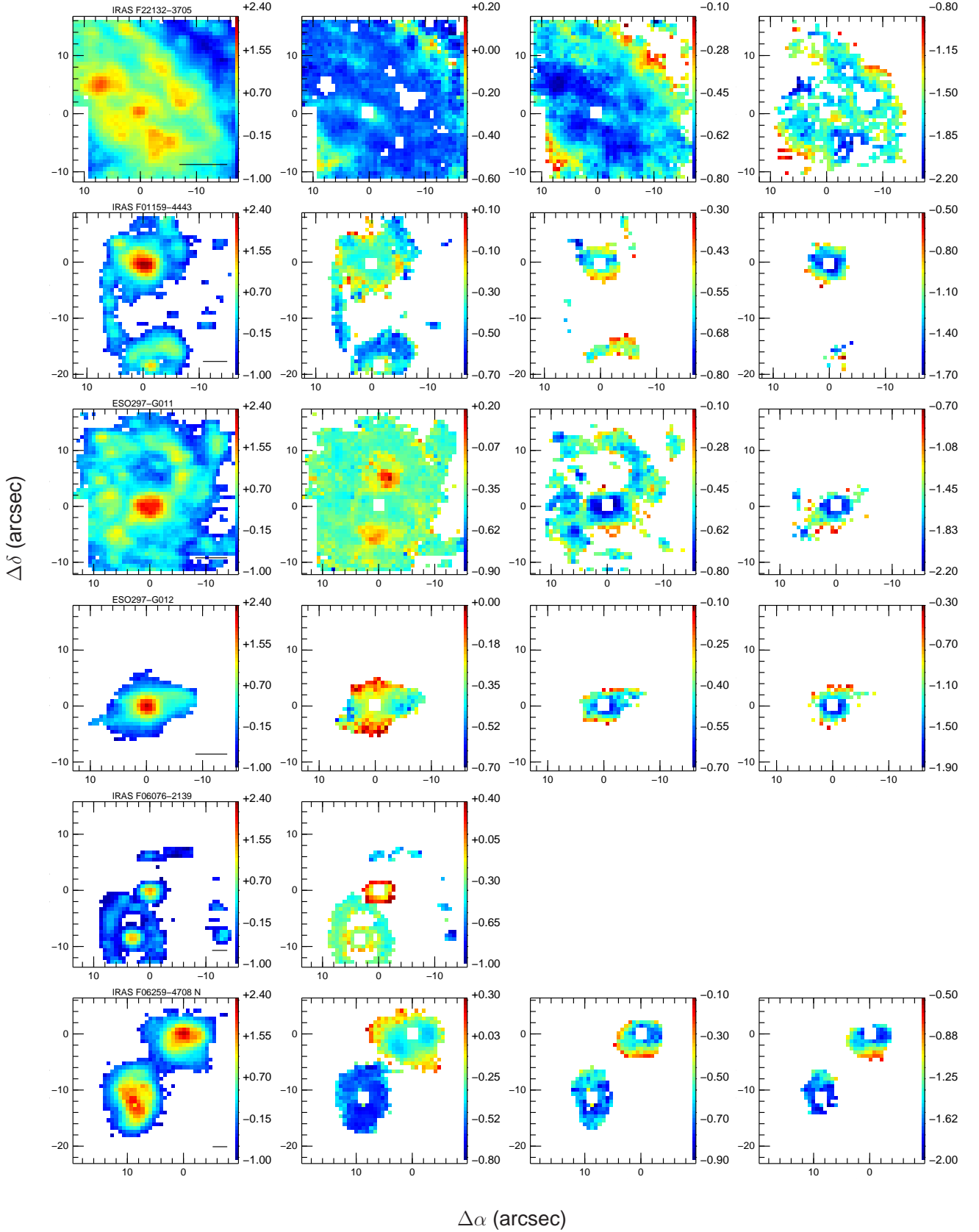


Fig. 2. continued.

mergers, the distribution of the emission line ratios for the entire sample of LIRGs was divided into three main groups according to their morphology: isolated, interacting, and merger remnants.

The  $[\text{N II}]\lambda 6584/\text{H}\alpha$ ,  $[\text{S II}]\lambda\lambda 6717, 6731/\text{H}\alpha$ , and  $[\text{O I}]\lambda 6300/\text{H}\alpha$  emission line ratio distributions for these classes of galaxies as well as for the entire sample are shown in Fig. 3. Galaxies with

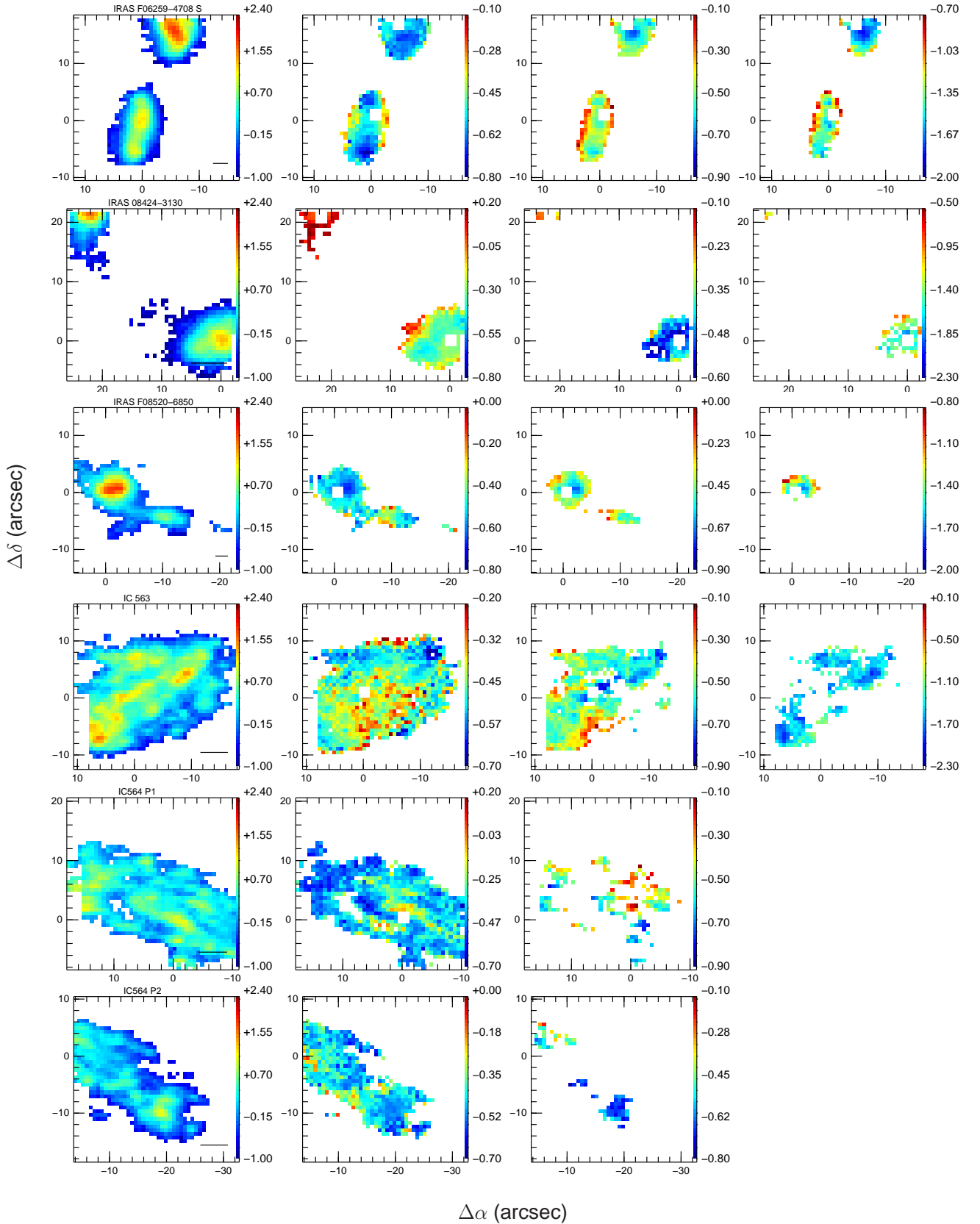
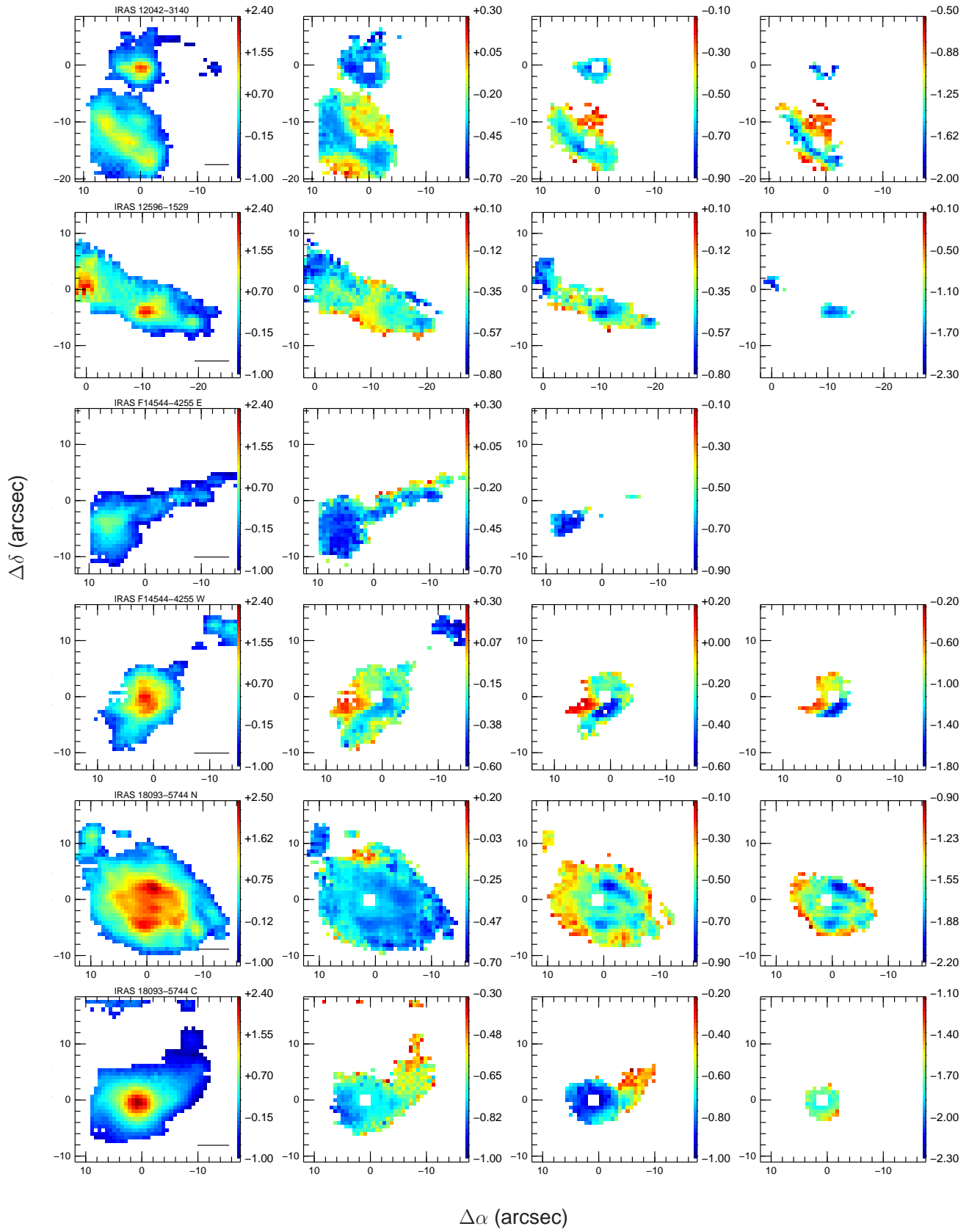


Fig. 2. continued.

dubious classification (see Table 1) were excluded from the histograms or the individual groups. The number of data points as well as the median and standard deviation of these distribu-

tions are indicated in Table 2. We also indicate in each panel the boundaries between ionization caused by stars and by other mechanisms in the Baldwin et al. (1981, hereafter BPT) dia-


**Fig. 2.** continued.

grams according to the boundaries proposed by different authors. The original boundaries (Veilleux & Osterbrock 1987) were empirically determined using a sample that includes extragalactic

$H\ II$  regions, and nuclear (or integrated) data for starburst galaxies and different kinds of active galaxies (i.e. Seyfert 2, LINERs, narrow-line radio galaxies and what would be called today “in-

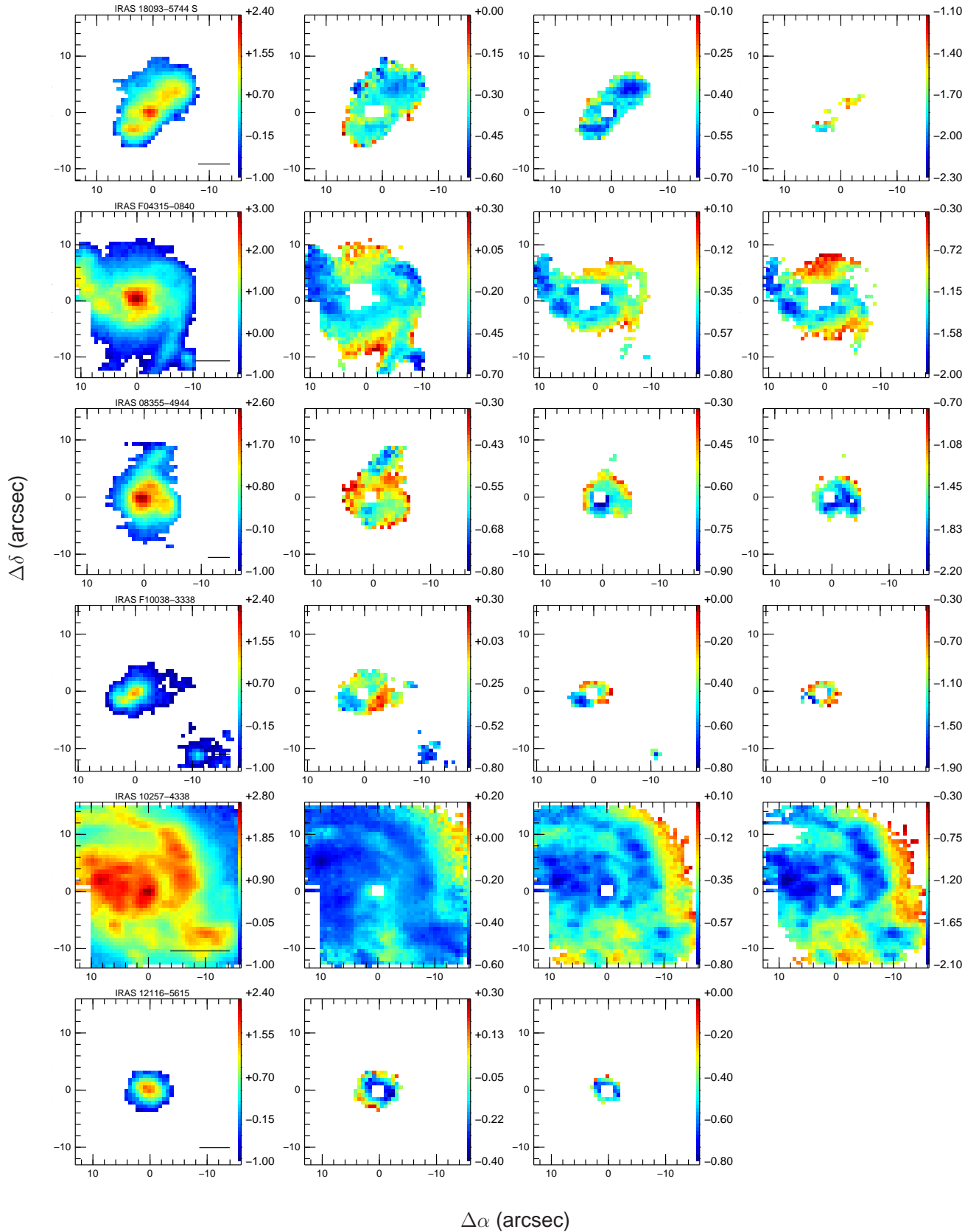


Fig. 2. continued.

intermediate objects”). Despite a recent new discussion about the location of these boundaries, we considered that they provide valuable information because i) they are the only set of *empir-*

*ical* boundaries for the *three* BPT diagnostic diagrams ii) they facilitate a possible comparison of the line ratios presented here with those in previous works. The other complete set of three

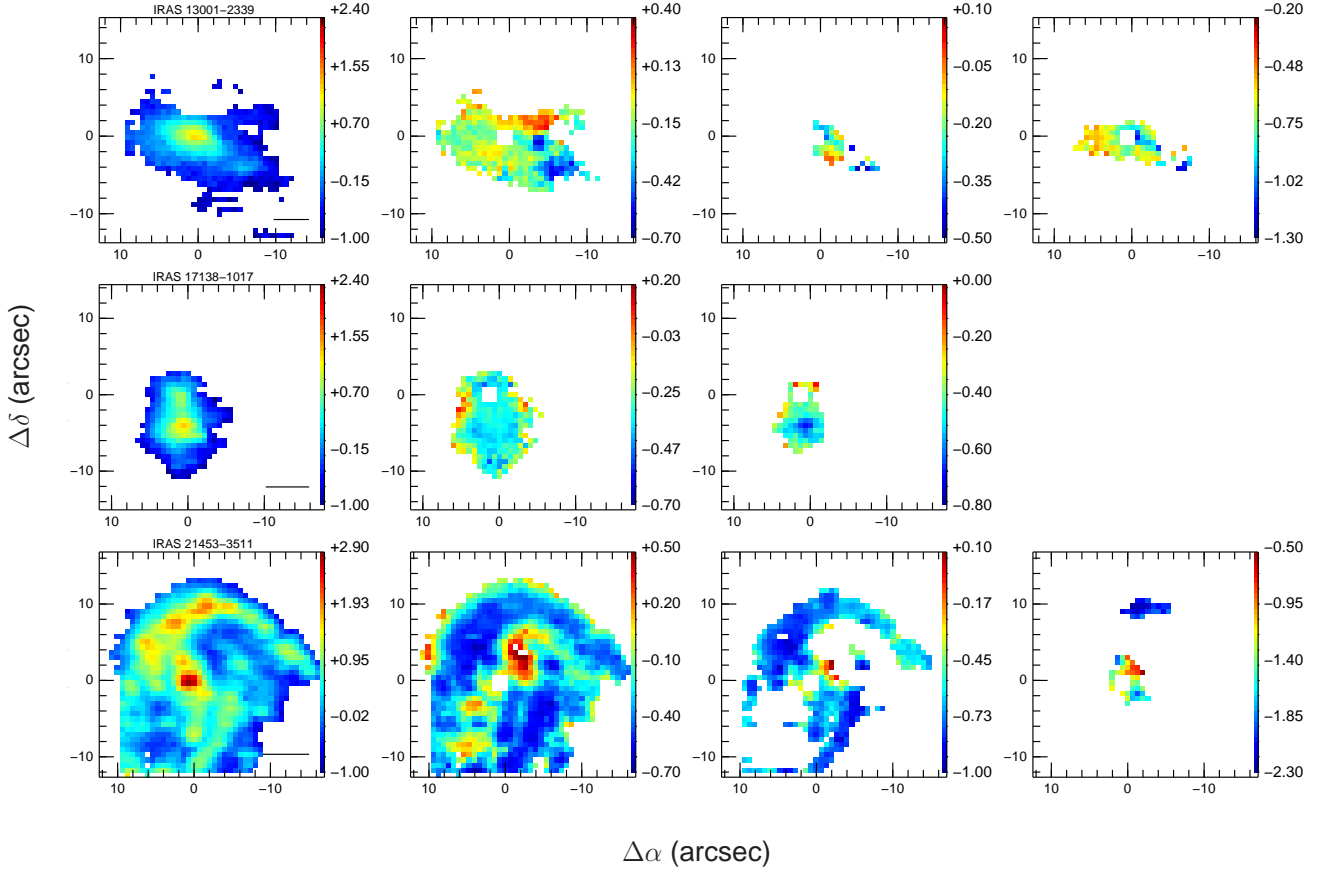


Fig. 2. continued.

boundaries is the one proposed by Kewley et al. (2001b). Using a combination of photo-ionization and stellar populations synthesis models the extreme cases under which line ratios can be explained via photo-ionization caused by stars. Recently, the empirical borders associated to the  $[\text{N II}]\lambda 6584/\text{H}\alpha$  line ratio have been up-dated by using the *Sloan Digital Sky Survey* (hereafter SDSS, York et al. 2000) data (Kauffmann et al. 2003; Stasińska et al. 2006). There is no similar up-date for the diagnostic diagrams involving the  $[\text{S II}]\lambda\lambda 6717, 6731/\text{H}\alpha$  and the  $[\text{O I}]\lambda 6300/\text{H}\alpha$  line ratios.

In order to locate the ionization type boundaries in Fig. 3 we assumed a  $\log([\text{O III}]\lambda 5007/\text{H}\beta) = -0.2$ . This is the median observed value for the sample of LIRGs sample presented in Alonso-Herrero et al. (2009). Individual values range between  $-0.6$  and  $0.1$ <sup>1</sup> (excluding NGC 7469, which is known to host a luminous Seyfert 1 nucleus that largely affects its integrated spectrum). As is illustrated in Fig. 3 with gray bands, the boundaries change very little in this  $[\text{O III}]\lambda 5007/\text{H}\beta$  range (typically  $\sim 0.1$  dex for the empirical boundaries of Veilleux & Osterbrock (1987), Stasińska et al. (2006) and Kauffmann et al. (2003) and  $\sim 0.2$  dex for the theoretical boundaries of Kewley et al. (2001b)) making this  $\log([\text{O III}]\lambda 5007/\text{H}\beta) = -0.2$ , a reasonable assumption for establishing the *mean* borders.

The line ratio distributions for the whole sample (Fig. 3, upper row) are not symmetrical around a mean value, but

show a significant wing towards high values. This suggests that a fraction of regions have a relatively high ionization (i.e. LINER-like). According to the Veilleux & Osterbrock boundaries, the percentage of data presenting a LINER spectrum corresponds to 19%, 31%, and 35% when using the  $[\text{N II}]\lambda 6584/\text{H}\alpha$ ,  $[\text{S II}]\lambda\lambda 6717, 6731/\text{H}\alpha$ , and  $[\text{O I}]\lambda 6300/\text{H}\alpha$ , respectively. Using the boundaries proposed by Kewley et al. (2001b), the number of spaxels that cannot be explained as purely ionized by stars is significantly smaller (4%, 2%, and 25%, for the  $[\text{N II}]\lambda 6584/\text{H}\alpha$ ,  $[\text{S II}]\lambda\lambda 6717, 6731/\text{H}\alpha$ , and  $[\text{O I}]\lambda 6300/\text{H}\alpha$  line ratios, respectively). The significant differences in the percentages when comparing the three line ratios could be due to the fact that these distributions do not come from exactly the same regions (i.e. set of spectra). Indeed, the  $[\text{O I}]\lambda 6300/\text{H}\alpha$  and  $[\text{S II}]\lambda\lambda 6717, 6731/\text{H}\alpha$  data points are restricted to a smaller region than the  $[\text{N II}]\lambda 6584/\text{H}\alpha$  ones because the  $[\text{O I}]$  and  $[\text{S II}]$  lines have on average lower S/N than the  $[\text{N II}]$  line. However, when these distributions are generated with data points from the same regions for the three lines (not shown), we find similar differences between the percentages when using the Kewley et al. boundaries (1%, 1% and 13%) and even larger ones when using the Veilleux & Osterbrock boundaries (7%, 21% and 22% for the  $[\text{N II}]\lambda 6584/\text{H}\alpha$ ,  $[\text{S II}]\lambda\lambda 6717, 6731/\text{H}\alpha$ , and  $[\text{O I}]\lambda 6300/\text{H}\alpha$  line ratios, respectively). This confirms that the  $[\text{O I}]\lambda 6300/\text{H}\alpha$  distribution has a higher percentage of data points with high ionization than the other two distributions. That the  $[\text{S II}]\lambda\lambda 6717, 6731$  and  $[\text{O I}]\lambda 6300$  emission is enhanced by shocks and therefore the  $[\text{S II}]\lambda\lambda 6717, 6731/\text{H}\alpha$  and, especially,  $[\text{O I}]\lambda 6300/\text{H}\alpha$  ratio are better tracers of shock-induced ionization (e.g. Dopita & Sutherland 1995) suggests a significant pres-

<sup>1</sup> These ratios have not been corrected for the underlying stellar absorption in  $\text{H}\beta$ . Such an absorption could typically decrease the  $[\text{O III}]\lambda 5007/\text{H}\beta$  line ratio by  $\sim 0.0-0.2$  dex (see Alonso-Herrero et al. 2009, for details).

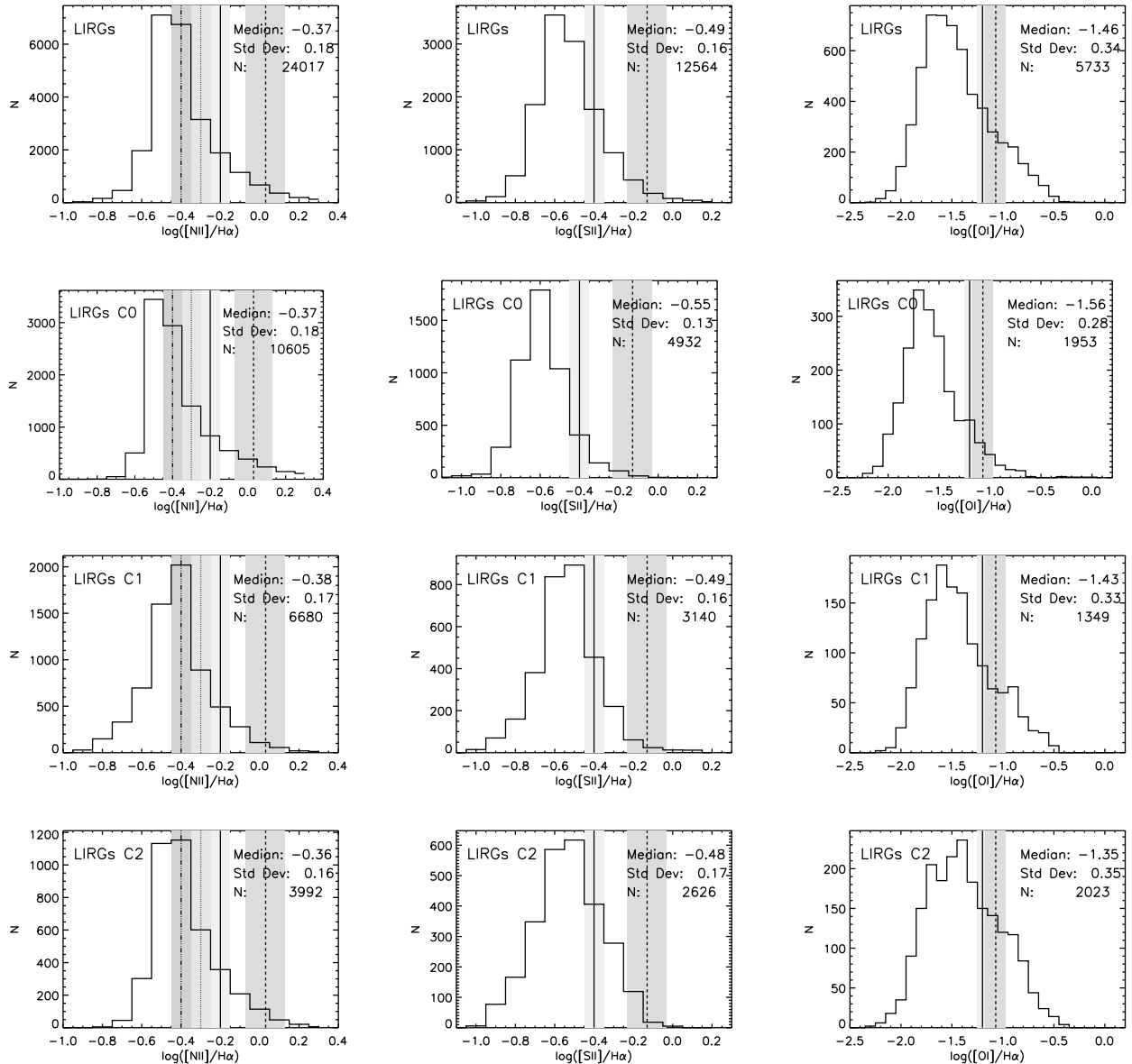


**Fig. 3.** Distributions of the different LIRG subsamples according  $[\text{N II}]\lambda 6584/\text{H}\alpha$ ,  $[\text{S II}]\lambda\lambda 6717, 6731/\text{H}\alpha$ , and  $[\text{O I}]\lambda 6300/\text{H}\alpha$  (first, second and third columns, respectively). Distributions are presented for the entire LIRG sample (1<sup>st</sup> row), for class 0 / isolated galaxies (2<sup>nd</sup> row), class 1 / interacting (3<sup>rd</sup> row), and class 2 / advanced mergers (4<sup>th</sup> row). The different vertical lines indicate the boundaries between ionization by stars and by other mechanisms proposed in different works and assuming a  $\log([\text{O III}]\lambda 5007/\text{H}\beta) = -0.2$ . The code used is: continuous line - Veilleux & Osterbrock (1987); dotted line - Kauffmann et al. (2003); dashed line - Kewley et al. (2001b); three dots/dashed line - Stasińska et al. (2006). The gray bands show the variation of a given boundary when the assumed  $[\text{O III}]\lambda 5007/\text{H}\beta$  value changes the full range observed in the Alonso-Herrero et al. LIRGs sample (i.e. -0.6,0.1).

ence of this type of ionization in the extra-nuclear extended regions of LIRGs. This will be explored in more detail below.

A clear distinction emerges in the excitation properties, i.e. in the distributions of the emission line ratios, when LIRGs are separated according to their interaction class (Fig. 3). While the  $[\text{N II}]\lambda 6584/\text{H}\alpha$  line ratio distributions are similar with a median ratio of  $\sim -0.37 \pm 0.18$  dex, typical of H II, the  $[\text{S II}]\lambda\lambda 6717, 6731/\text{H}\alpha$  line ratio shows on average higher values, i.e. higher excitation, in the more dynamically perturbed systems (class 1 and 2). Indeed, median( $\pm$ standard deviation) values of  $-0.55 \pm 0.13$ ,  $-0.49 \pm 0.16$ , and  $-0.48 \pm 0.17$  are found for classes 0, 1, and 2, respectively. Similar values are found after

assuming a correction for a H $\alpha$  component in absorption with an equivalent width of  $2\text{\AA}$ .

A more extreme change is evident in the  $[\text{O I}]\lambda 6300/\text{H}\alpha$  ratio (i.e. shock tracer) with median values of  $-1.56 \pm 0.28$ ,  $-1.43 \pm 0.33$ , and  $-1.35 \pm 0.35$  for classes 0, 1, and 2, respectively. In addition, LIRGs belonging to both classes 1 and 2 seem to have a double-peak distribution, with values around -1.4 (i.e. H II-like) and -0.9 (LINER-like). In all the cases, the Kolmogorov-Smirnoff test allows us to reject the possibility that these distributions come from the same parent distribution even in the case of the  $[\text{N II}]\lambda 6584/\text{H}\alpha$  line ratio.

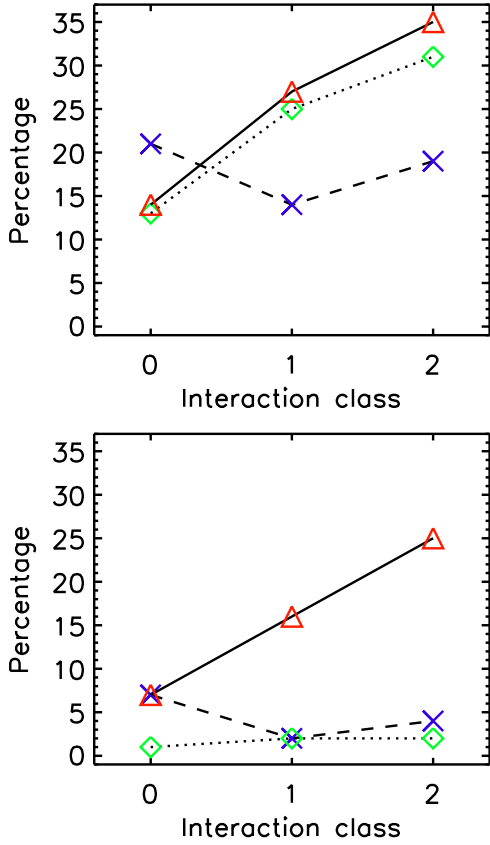


**Fig. 4.** Percentage of data for the different interaction classes classified as LINERs using the Veilleux & Osterbrock (1987) line ratio boundaries (up) and Kewley et al. (2001b) ones (down) and assuming  $[\text{O III}]\lambda 5007/\text{H}\beta = -0.2$ . Measured values are indicated with crosses, diamonds and triangles for the  $[\text{N II}]\lambda 6584/\text{H}\alpha$ ,  $[\text{S II}]\lambda\lambda 6717, 6731/\text{H}\alpha$ , and  $[\text{O I}]\lambda 6300/\text{H}\alpha$  line ratios respectively. Data corresponding to the different interaction class have been joined with dashed, dotted and continuous lines, respectively for an easier reading of the figure.

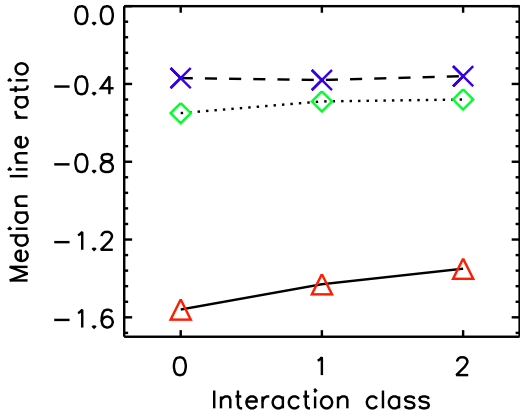


**Fig. 5.** Variation of the median of the average line ratio per galaxy with the interaction class. We use the same line and color code as in Fig. 4 to distinguish among the emission line ratios.

Moreover, when using the Veilleux & Osterbrock boundaries the percentage of data points with  $[\text{S II}]\lambda\lambda 6717, 6731/\text{H}\alpha$  and  $[\text{O I}]\lambda 6300/\text{H}\alpha$  line ratios in the LINER range increases by factors of two and three with the interaction class with respect to the

isolated galaxies (class 0), representing about  $\sim 17\%$  and  $\sim 33\%$  of the regions in class 1 and 2 galaxies, respectively. When using the Kewley et al. boundaries, only the percentage for the  $[\text{O I}]\lambda 6300/\text{H}\alpha$  line ratio shows a significant increase (see Fig. 4).

As shown in Table 1, the number of data points associated with a galaxy can range from a few tens to a few thousands, depending on the line ratio. Given this range of two orders of magnitude, one might wonder if the distributions presented in Fig. 3 are biased due to the contribution of a few galaxies. To check this possibility, we generated the distributions for the three line ratios and the different morphological groups, but without the pointing with the largest number of spaxels. These were IRAS F22132–3705 for class 0, ESO 297–G011 for class 1, and IRAS 10257–4338 for class 2. In this way, the remaining pointings contribute in a similar manner to the distribution (i.e. with several hundreds of data points for the  $[\text{N II}]\lambda 6584/\text{H}\alpha$  line ratio in most of the cases and with many tens - a few hundreds for the  $[\text{S II}]\lambda\lambda 6717, 6731/\text{H}\alpha$  and  $[\text{O I}]\lambda 6300/\text{H}\alpha$  line ratios). The distributions (not shown here) were similar to those for the whole sample, with differences between the medians  $\sim 0.05$  dex. Moreover, we checked how the median of the average line ratios per galaxy changes with the interaction class. This is shown in Fig. 5. In this way, every pointing contributes with one data point per line ratio. As was found for the data distributions, this figure shows how, while the  $[\text{N II}]\lambda 6584/\text{H}\alpha$  line ratio remains constant with the interaction class, the  $[\text{S II}]\lambda\lambda 6717, 6731/\text{H}\alpha$  and, especially, the  $[\text{O I}]\lambda 6300/\text{H}\alpha$  line ratio increases with the degree of interaction.

Although it would have been interesting to compare the present line ratio distributions with those obtained for other kinds of galaxies (e.g. normal spirals, less powerful starbursts), there is a clear lack of data comparable to those presented here. In particular, a meaningful comparison requires galaxies with line ratios measured at similar spatial scales as those sampled here. For example, line ratios derived for the SDSS<sup>2</sup>, the largest extragalactic survey up to date, were derived from spectra obtained through 3-arcsec diameter fibers. For galaxies at similar redshift like the present sample, this would be representative of the ionization in the *nuclear* regions, and thus, not directly comparable with our analysis on the external areas. For galaxies at larger distances - say,  $0.04 < z < 0.10$  - the spatial sampling in the SLOAN galaxies would be much larger ( $\varnothing \sim 2.4 - 5.4$  kpc) and thus again not directly comparable. The only galaxy with published data comparable to those presented here is the spiral NGC 5194 (also known as *Whirlpool Galaxy*, Blanc et al. 2009), a spiral galaxy interacting with a dwarf galaxy. At its distance ( $\sim 8$  Mpc) and with the size of the VIRUS-P fibers ( $\varnothing \sim 4''.3$ ) the spatial sampling is comparable with that for our sample within a factor of  $\sim 3$ . Figure 6 shows the distribution for the two available line ratios for this galaxy. While the  $[\text{N II}]\lambda 6584/\text{H}\alpha$  distributions for the LIRGs and NGC 5194 are similar, LIRGs have larger  $[\text{S II}]\lambda\lambda 6717, 6731/\text{H}\alpha$  ratios. Because this comparison was done only with one galaxy, this result needs to be revised when line ratios in the external areas of larger samples of spiral galaxies at similar linear spatial resolution become available.

### 3.3. Anti-correlation between excitation and $\text{H}\alpha$ luminosity

Maps presented in Sect. 3.1 (Fig. 2) display an increase on the line ratio in those areas with low  $\text{H}\alpha$  surface brightness. Similar results have been observed in other environments, like

<sup>2</sup> See <http://www.mpa-garching.mpg.de/SDSS/>.

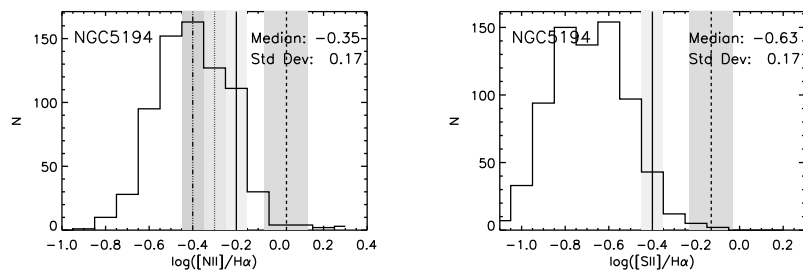


**Fig. 6.** Same as Fig. 3 for NGC 5194 (only  $[\text{N II}]\lambda 6584/\text{H}\alpha$  and  $[\text{S II}]\lambda\lambda 6717,6731/\text{H}\alpha$  line ratios).

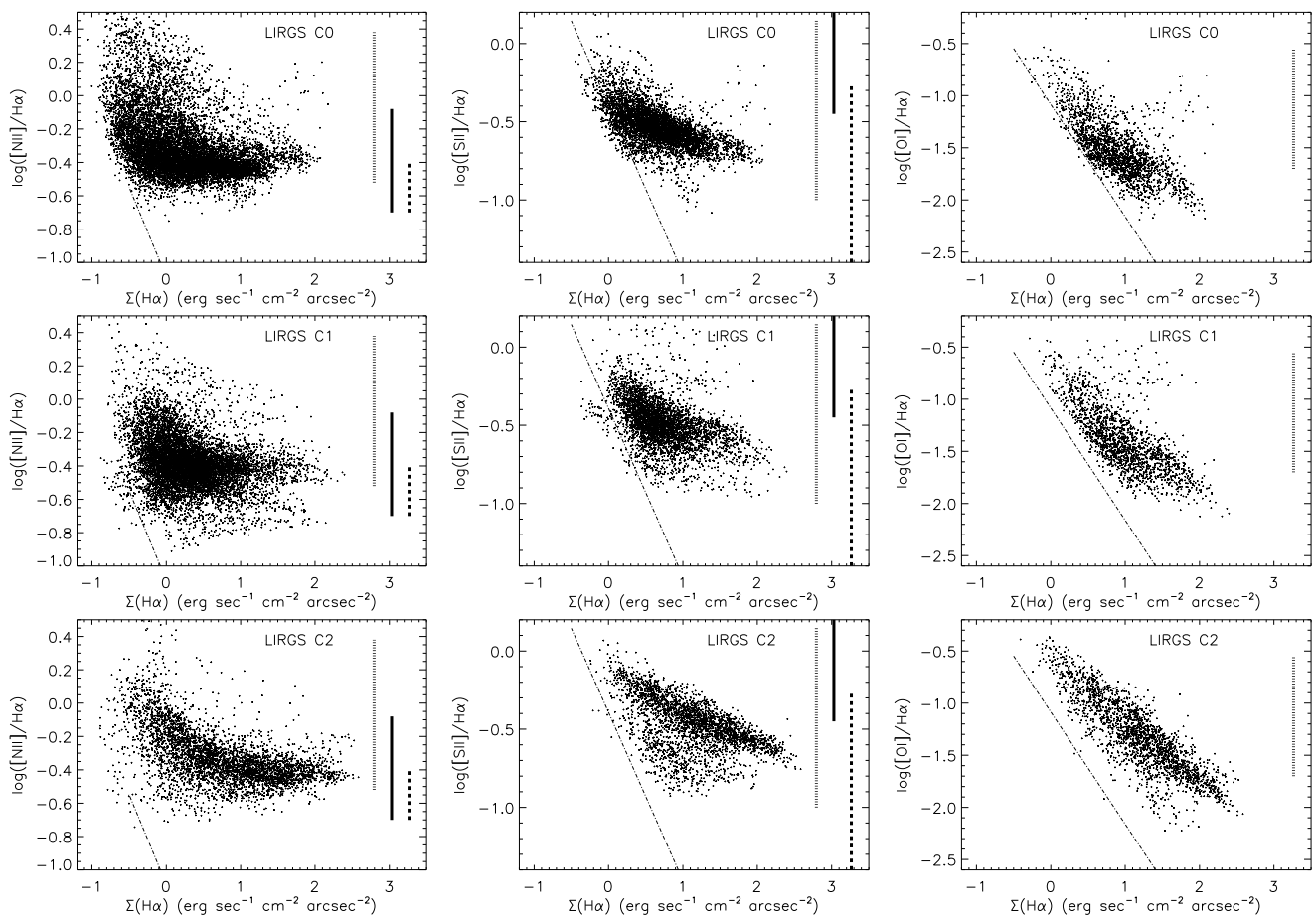


**Fig. 7.** Relation between the  $\text{H}\alpha$  surface brightness and the  $[\text{N II}]\lambda 6584/\text{H}\alpha$  (left),  $[\text{S II}]\lambda\lambda 6717,6731/\text{H}\alpha$  (middle), and  $[\text{O I}]\lambda 6300/\text{H}\alpha$  (right). Units are in an arbitrary scaling. The dashed (continuous) vertical bars represent the covered line ratio ranges for the sample of galactic  $\text{H II}$  regions (DIG areas) studied by Madsen et al. (2006). Note that because its  $[\text{S II}]/\text{H}\alpha$  line ratio only includes the  $\lambda 6717$  sulfur line, we added an offset of 0.25 dex to their values to take into account the contribution from the  $\lambda 6731$  line. Also the line ratio ranges for the eDIG areas in a sample of nine edge-on spiral galaxies is shown with dotted line for comparison (Miller & Veilleux 2003). Dotted-dashed lines represent our estimated observational limits.

our Galaxy (Madsen et al. 2006; Reynolds et al. 1999), or other spiral galaxies (Collins & Rand 2001; Miller & Veilleux 2003; Blanc et al. 2009) in the so-called diffuse ionized gas (DIG) or warm interstellar medium (WIM). In this section we further explore this result by looking at the relation between the ionization degree and surface brightness for the different interaction groups. This is shown in Fig. 7, where each data point represents the information from an individual spaxel.

As can be seen in the figure, while the  $[\text{N II}]\lambda 6584/\text{H}\alpha$  covers almost three orders of magnitude in  $\text{H}\alpha$  surface brightness, the  $[\text{S II}]\lambda\lambda 6717,6731/\text{H}\alpha$  and the  $[\text{O I}]\lambda 6300/\text{H}\alpha$  line ratios are restricted to only about two. Also, low values of  $[\text{S II}]\lambda\lambda 6717,6731/\text{H}\alpha$  and  $[\text{O I}]\lambda 6300/\text{H}\alpha$  are only found at high  $\text{H}\alpha$  surface brightness. We estimated our observational limit by looking at the typical values and uncertainties measured for our  $[\text{N II}]\lambda 6584/\text{H}\alpha$  line ratio. Then we allowed for a maximum un-

certainty in the logarithm of the line ratios of 0.4 and assumed that the S/N scales with the root square of the signal. The derived observational limit is shown in Fig. 7 which shows how these effects are caused by the sensitivity limit of the data, as was pointed out in Sect. 3.1. That is, the relatively low S/N of the  $[\text{S II}]\lambda\lambda 6717,6731$  and  $[\text{O I}]\lambda 6300$  emission lines in the outer parts prevent us from measuring low  $[\text{S II}]\lambda\lambda 6717,6731/\text{H}\alpha$  and  $[\text{O I}]\lambda 6300/\text{H}\alpha$  line ratios at low  $\text{H}\alpha$  surface brightness. Figure 7 shows that independently of the line ratio, high values are found at low surface brightness as it happened in our Galaxy and other spiral galaxies. Moreover, typical distances where the high line ratios are found (from  $\sim 400$  pc up to  $\sim 6$  kpc) are comparable with the distances where this anti-correlation between excitation and surface brightness has been found (up to  $\sim 8$  kpc Collins & Rand 2001; Miller & Veilleux 2003).

The figure also shows the ranges of  $[\text{N II}]\lambda 6584/\text{H}\alpha$  and  $[\text{S II}]\lambda\lambda 6717,6731/\text{H}\alpha$  line ratios measured in a sample of  $\text{H II}$  regions and DIGs areas in our Galaxy by Madsen et al. (2006), as well as for extragalactic DIG (Miller & Veilleux 2003). Part of the  $[\text{N II}]\lambda 6584/\text{H}\alpha$  and  $[\text{S II}]\lambda\lambda 6717,6731/\text{H}\alpha$  line ratios are compatible with those expected for  $\text{H II}$  regions. However, there is a large number of spaxels with line ratios similar to what it is observed in the DIGs areas.

$\text{H II}$  regions are generally understood as photo-ionized by the young stellar populations within them. On the other hand, DIGs seem more difficult to explain only via photo-ionization (e.g. Miller & Veilleux 2003). If they are interpreted only as photo-ionization areas, there is a need for extra heating (Reynolds et al. 1999; Mathis 2000) and even with this extra heating, it is difficult to reach  $[\text{N II}]\lambda 6584/\text{H}\alpha \gtrsim 1$  line ratios. Another possibility would be that these line ratios are the composite effect of photo-ionization and shocks or turbulent mixing layers (TML, Collins & Rand 2001; Miller & Veilleux 2003). In the next section we will explore the role of these different ionization mechanisms by comparing our measured line ratios with the predictions of the models.

### 3.4. Ionization mechanisms in the extra-nuclear ionized regions: young stars and shocks

To investigate the nature of the ionization mechanisms present in the extended extra-nuclear regions, the  $[\text{S II}]\lambda\lambda 6717,6731/\text{H}\alpha$  vs.  $[\text{N II}]\lambda 6584/\text{H}\alpha$  and  $[\text{O I}]\lambda 6300/\text{H}\alpha$  vs.  $[\text{N II}]\lambda 6584/\text{H}\alpha$  diagnostic diagrams for (thousands) of data points sampling these regions were compared with model predictions for  $\text{H II}$  regions, shocks and AGNs. State-of-the-art models for evolving  $\text{H II}$  regions (Dopita et al. 2006), shocks (Allen et al. 2008), TML (Slavin et al. 1993) and dusty AGNs (Groves et al. 2004) covering a wide range of physical parameters (ionization, density, stellar ages, shock velocity, etc.) and metallicities were considered. The results for the galaxies were separated according to their interaction class, and set of models best representing the data are given in Figs. 8 and 9 for the  $[\text{S II}]\lambda\lambda 6717,6731/\text{H}\alpha$  vs.  $[\text{N II}]\lambda 6584/\text{H}\alpha$  and  $[\text{O I}]\lambda 6300/\text{H}\alpha$  vs.  $[\text{N II}]\lambda 6584/\text{H}\alpha$  diagnostic diagrams, respectively. Galaxies with dubious classification (see Table 1) were excluded. The data associated with each individual pointing have been attached as *On-line Material*.

From these diagrams it is clear that although the ionization properties of most of the extended, extra-nuclear regions are consistent with those of  $\text{H II}$  regions, there is a trend with the interaction class. As the interaction progresses (e.g. moving from class 0 to class 2), a larger fraction of extra-nuclear regions shows a clear shift towards an increased excitation, as traced by the in-

crement of the  $[\text{S II}]\lambda\lambda 6717,6731$  and, in particular,  $[\text{O I}]\lambda 6300$  emission with respect to  $\text{H}\alpha$  (see Figs. 8 and 9).

Although individual galaxies within an interaction class or regions within galaxies can behave differently, a direct comparison of all the available data (represented by thousands of points in the diagrams of Figs. 8 and 9) with the model predictions allow us to obtain some general conclusions about the ionization mechanisms playing the main role in the extra-nuclear regions of LIRGs.

The first conclusion that can be drawn from a comparison of Figs. 8 and 9 is that TML are not playing a major role in the ionization of the extra-nuclear regions of this sample. Models can marginally reproduce the observed  $[\text{N II}]\lambda 6584/\text{H}\alpha$  vs.  $[\text{S II}]\lambda\lambda 6717,6731/\text{H}\alpha$ , but clearly under-predict the  $[\text{O I}]\lambda 6300/\text{H}\alpha$  line ratio for a given  $[\text{N II}]\lambda 6584/\text{H}\alpha$ .

Instead, most of the regions are consistent with ionization by young stellar populations with ages of 3 Myr or less and metallicities twice solar. The measured  $\text{H}\alpha$  emission line equivalent widths in these regions are in the 40 to 300 Å range (Rodríguez-Zaurín et al. in prep.), and therefore do not correspond with the strong  $\text{H}\alpha$  lines (equivalent widths of 1000 to 2000 Å) expected in very young ( $\leq 3$  Myr) stellar clusters (STARBURST99, Leitherer et al. 1999). This apparent discrepancy is likely due to contamination by evolved stellar populations (see Alonso-Herrero et al. 2010). Because the physical scale of each resolution element (determined by a seeing of  $\sim 1''.2$ ) would be about 480 pc, the measured equivalent widths are likely the result of different stellar populations where the old stars present in these regions contribute to the optical continuum, but not to the emission lines. Moreover, typical sizes for giant  $\text{H II}$  regions would be  $\lesssim 400$  pc (e.g. Kennicutt 1984; Alonso-Herrero et al. 2002). Because our typical resolution is slightly higher, a single spaxel can sample both pure DIG and regions of very young star formation. This implies that measured line ratios, specially the  $[\text{N II}]\lambda 6584/\text{H}\alpha$  one, are higher than those for pure  $\text{H II}$  regions and thus a comparison with models suggests too young stellar populations.

For regions showing a  $\log([\text{S II}]\lambda\lambda 6717,6731/\text{H}\alpha) \gtrsim -0.6$ , the model predictions considering ionization mechanisms different from the TML's ones overlap and therefore no firm conclusions can be made based on the  $[\text{S II}]\lambda\lambda 6717,6731/\text{H}\alpha$  vs.  $[\text{N II}]\lambda 6584/\text{H}\alpha$  alone (see Fig. 8). However, much of this overlap disappears when the  $[\text{O I}]\lambda 6300/\text{H}\alpha$  ratio is considered. In particular regions showing  $\log([\text{O I}]\lambda 6300/\text{H}\alpha) \geq -1.6$  are best explained by the presence of shocks with velocities of less than 200 km s<sup>-1</sup> and metallicities 1-2 solar (see Fig. 9).

We note that a detailed comparison of our data with the models in Figs. 8 and 9 may lead to some inconsistencies. For instance, the  $[\text{S II}]\lambda\lambda 6717,6731/\text{H}\alpha$ -  $[\text{N II}]\lambda 6584/\text{H}\alpha$  diagram presents less data points in the area of shocks of  $v_s \sim 200 - 300$  km s<sup>-1</sup> than the  $[\text{O I}]\lambda 6300/\text{H}\alpha$ -  $[\text{N II}]\lambda 6584/\text{H}\alpha$  diagram. These disagreements may be due to the intrinsic difficulty in modeling some emission (e.g.  $[\text{O I}]\lambda 6300$  line Dopita & Sutherland 1995) as well as possible observational effects. The areas sampled by a given spaxel include both star-forming regions and diffuse ionized gas, which affect the line ratios differently. In any case, these figures should be read looking for general behaviors rather than for detailed comparisons.

Taking this into account, we considered the  $[\text{O I}]\lambda 6300/\text{H}\alpha$ -  $[\text{N II}]\lambda 6584/\text{H}\alpha$  diagram as our main indicator to establish the most important ionization mechanism for individual galaxies in Table 3. In some cases this was complemented with other indicators, especially for the galaxies with no  $[\text{O I}]\lambda 6300$  detections.

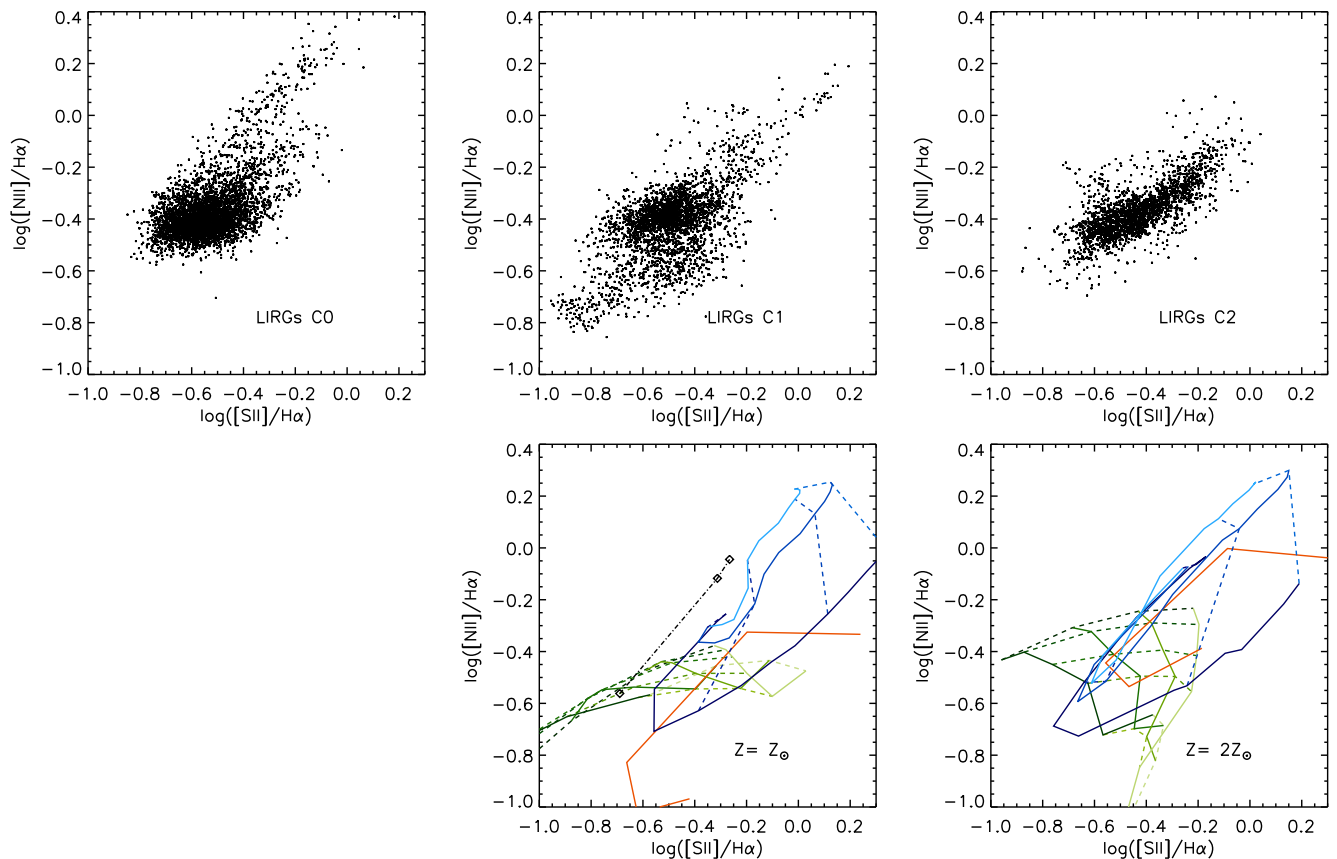


**Fig. 8.**  $[\text{S II}]\lambda\lambda 6717,6731/\text{H}\alpha$  vs.  $[\text{N II}]\lambda 6584/\text{H}\alpha$  diagrams. *First row:* Line ratios for the different LIRGs groups in our sample. *Second row:* Theoretical models used for comparison where those in the middle column have solar metallicity and those in the right twice solar metallicity. In all panels, the empirical boundaries proposed in Veilleux & Osterbrock (1987) to separate the ionization by stars or other mechanisms assuming a  $\log([\text{O III}]\lambda 5007/\text{H}\beta) = -0.2$  are shown. The color code for the models is: i) *Green scale:* Star-formation models from Dopita et al. (2006). Different solid lines represent different  $R$  parameter which vary from 0 (darkest green) to  $-6$  (lightest green) while dashed lines connect points with the same age ranging from 0.5 Myr (darkest green) to 3.0 Myr (lightest green); ii) *Orange scale:* Dusty AGN models from Groves et al. (2004). Ionization parameter ranges from 0.0 (bottom) to  $-4.0$  (rightmost edge). Only the cases with  $\alpha = -2.0$  have been plotted. Smaller  $\alpha$  parameters typically predict higher  $[\text{S II}]\lambda\lambda 6717,6731/\text{H}\alpha$  and  $[\text{N II}]\lambda 6584/\text{H}\alpha$  line ratios for a given ionization parameter. iii) *Blue scale:* Models for shocks without precursor from Allen et al. (2008) for  $n_e = 1 \text{ cm}^{-3}$ . Solid lines indicate models for magnetic parameters of  $B/n^{1/2} = 0$  (darkest blue), 2, and  $4 \mu\text{G cm}^{3/2}$  (lightest blue) while dashed lines joint points with velocities of  $100 \text{ km s}^{-1}$  (darkest blue),  $200 \text{ km s}^{-1}$  (medium blue) and  $300 \text{ km s}^{-1}$  (lightest blue). The predictions for models with shock velocities greater than  $300 \text{ km s}^{-1}$  occupy a similar area as those for  $v_s = 300 \text{ km s}^{-1}$  in this diagram. Models for shocks with precursor cover a similar area in this diagram displaced by  $\sim -0.2$  dex in both line ratios. iv) *Black dash-dotted line:* Models for turbulent mixing layers of Slavin et al. (1993) for  $Z = Z_\odot$  and transverse velocity  $v_t = 25 \text{ km s}^{-1}$ . Average temperature for the gas increase with  $[\text{N II}]\lambda 6584/\text{H}\alpha$ . The three diamonds indicates  $\log T = 5.0, 5.3$  and  $5.5$ .

Elevated line ratios can in principle be explained by both shocks and AGN. This is evident from the models presented in Figs. 8 and 9, as well as from integrated data from the literature (Kewley et al. 2006). Indeed, four of the 32 galaxies are classified as Seyfert (the northern member of IRAS F07027-6011, IRAS F13229-2934, and the western member of IRAS 14544-4255 and IRAS 21453-3511, see footnotes in Table 3). The northern member of IRAS F07027-6011 should not pose a problem, because most of its line ratios are typical of young stars. However, as stated in Table 3, some areas with elevated line ratios could be caused by the nuclear AGN. The galaxy IRAS 13229-3934 contains a central AGN which causes an ionization cone in the north-south direction (Bedregal et al. 2009). However, our measured line ratios are associated to wide areas in the *inter-arms* zone, not coincident with the direction of the ionization cone, and thus difficult to be explained by the cen-

tral AGN. Finally, for the western member IRAS 14544-4255 and IRAS 21453-3511, it is not possible to discern with the present information whether the ionization in the external areas is caused by shocks or the central AGN. However, an indirect argument allows us to favor shocks against AGN as the mechanisms responsible of the observed line ratios. As was shown for Arp 299, a very nearby LIRG, the extra-nuclear area with an excitation caused by the AGN (as seen by the  $[\text{O III}]\lambda 5007/\text{H}\beta$  line ratio) is very small and restricted to specific directions defined by the ionization cone (see detailed analysis for this system in García-Marín et al. 2006). Also, nuclear regions, where one could expect the largest influence of an AGN, were removed from our analysis (see Sect. 2.4).

It is worth mentioning that the metallicities (solar to twice solar) of the models (H II and shocks) that best fit the range of data are underabundant by a factor of  $\sim 1.5 - 2.0$  with respect

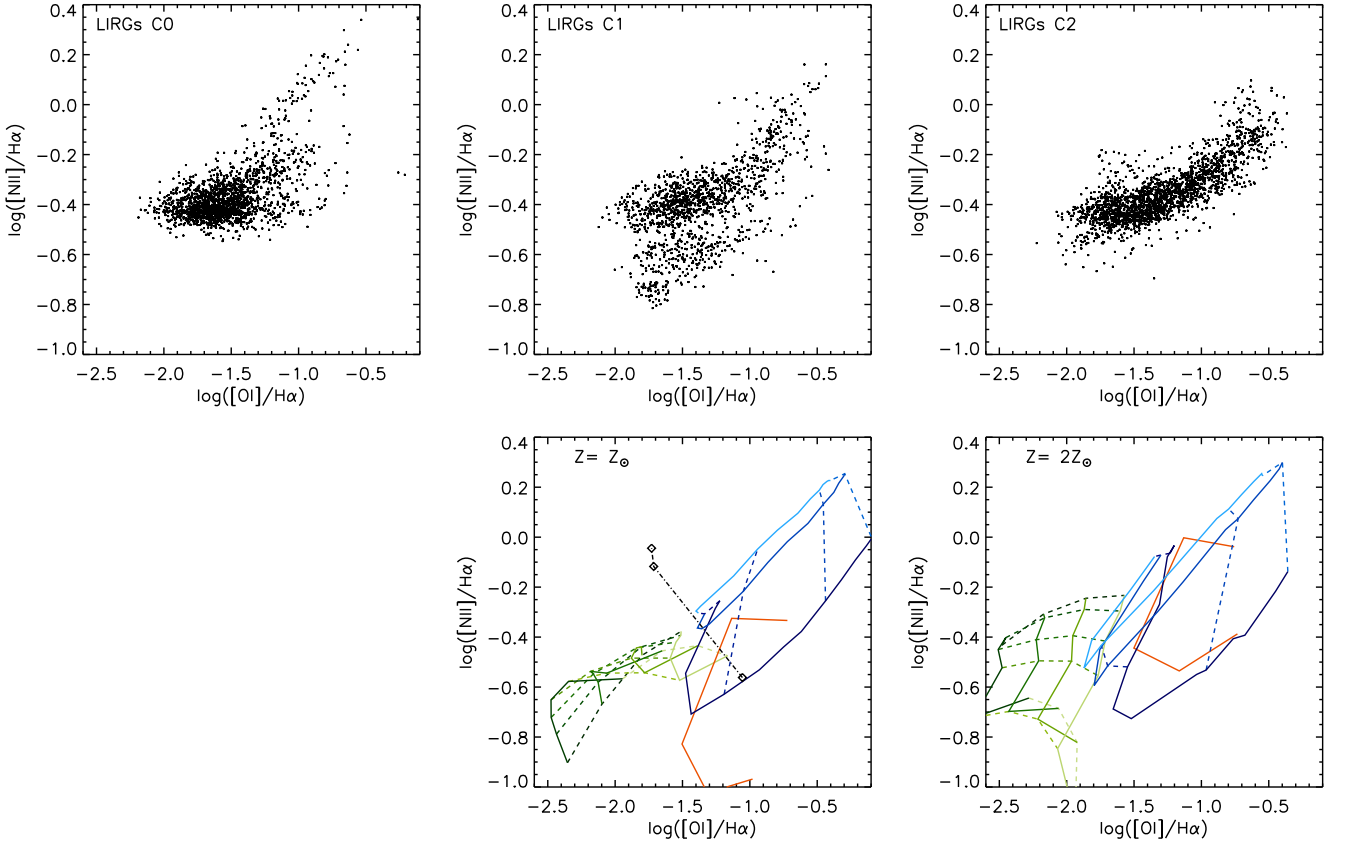


**Fig. 9.**  $[\text{O I}]\lambda 6300/\text{H}\alpha$  vs.  $[\text{N II}]\lambda 6584/\text{H}\alpha$  diagrams. *First row:* Line ratios for the different LIRGs groups in our sample. *Second row:* Theoretical models used for comparison where those in the middle column have solar metallicity and those in the right twice solar metallicity. The utilized color/symbol code is the same as in Fig. 8.

to what is expected from the mass-metallicity relation for galaxies (Tremonti et al. 2004). This relation predicts metallicities of  $Z \sim 1.9 - 2.8 Z_{\odot}^3$  for galaxies with masses as those expected in typical LIRGs ( $\sim 10^{10} - 10^{12} M_{\odot}$ , e.g., Hinz & Rieke 2006; Väisänen et al. 2008a,b). Similar findings for the nuclear region of these kinds of galaxies have been reported by Rupke et al. (2008).

In summary, the ionization of the extended, extra-nuclear regions in isolated galaxies (class 0), is mostly explained as due to young stars like in  $\text{H II}$  regions. Systems showing some degree of interaction (class 1 and 2) present a large and increasing fraction of regions which are better explained by shocks. This is particularly evident when using the the  $[\text{O I}]\lambda 6300/\text{H}\alpha$  vs.  $[\text{N II}]\lambda 6584/\text{H}\alpha$  diagnostic diagram. In particular cases (e.g. IRAS 21453–3511), an AGN also could explain the observed high line ratios. In order to explore the precise relevance of a putative AGN, other additional observables than those utilized here (e.g. flux in the  $[\text{O III}]\lambda 5007$  emission line) would be needed. Further evidence for the presence and relevance of shocks as ionizing sources can be found through the gas velocity dispersions and their correlations with the emission line ratios. This is presented in the next section.

### 3.5. The relation between excitation and gas velocity dispersion: further evidence for the importance of shocks

The presence and relevance of shocks in (U)LIRGs has already been suggested by a positive relation between the ionized gas velocity dispersion and its ionization degree as traced by the  $[\text{S II}]\lambda\lambda 6717, 6731/\text{H}\alpha$  ratio in a sample of about 30 galaxies (Armus et al. 1989; Dopita & Sutherland 1995; Veilleux et al. 1995). These studies were based on long-slit observations and were therefore dominated by the contribution from the high-surface brightness nuclear regions in a large number of cases. Also, the slit was positioned along a given orientation and therefore the results of these studies do not necessarily represent the excitation and kinematics of the ionized gas in the extra-nuclear extended (several kpc) regions. Instead, for the detailed study of the excitation conditions in the extended regions it is more appropriate to use the two-dimensional information provided by IFS data once the nuclear regions are removed, as already discussed for a small sample of ULIRGs (Monreal-Ibero et al. 2006). We performed a similar study with the present sample of LIRGs, limiting the analysis to the data with  $[\text{N II}]\lambda 6584/\text{H}\alpha$ ,  $[\text{S II}]\lambda\lambda 6717, 6731/\text{H}\alpha$ , and  $[\text{O I}]\lambda 6300/\text{H}\alpha$  higher than  $-0.7$ ,  $-0.8$ ,  $-1.8$ , respectively (i.e. line ratios in the range expected for shocks according to the models discussed in the previous section). In particular, Fig. 10 presents the relation between the excitation degree (here represented by our three line ratios) and the gas velocity dispersion for the entire sample (upper panels) and according interaction class (three lower panels).

<sup>3</sup> We have employed  $12 + \log(\text{O}/\text{H})_{\odot} = 8.66$ , from Asplund et al. (2004).

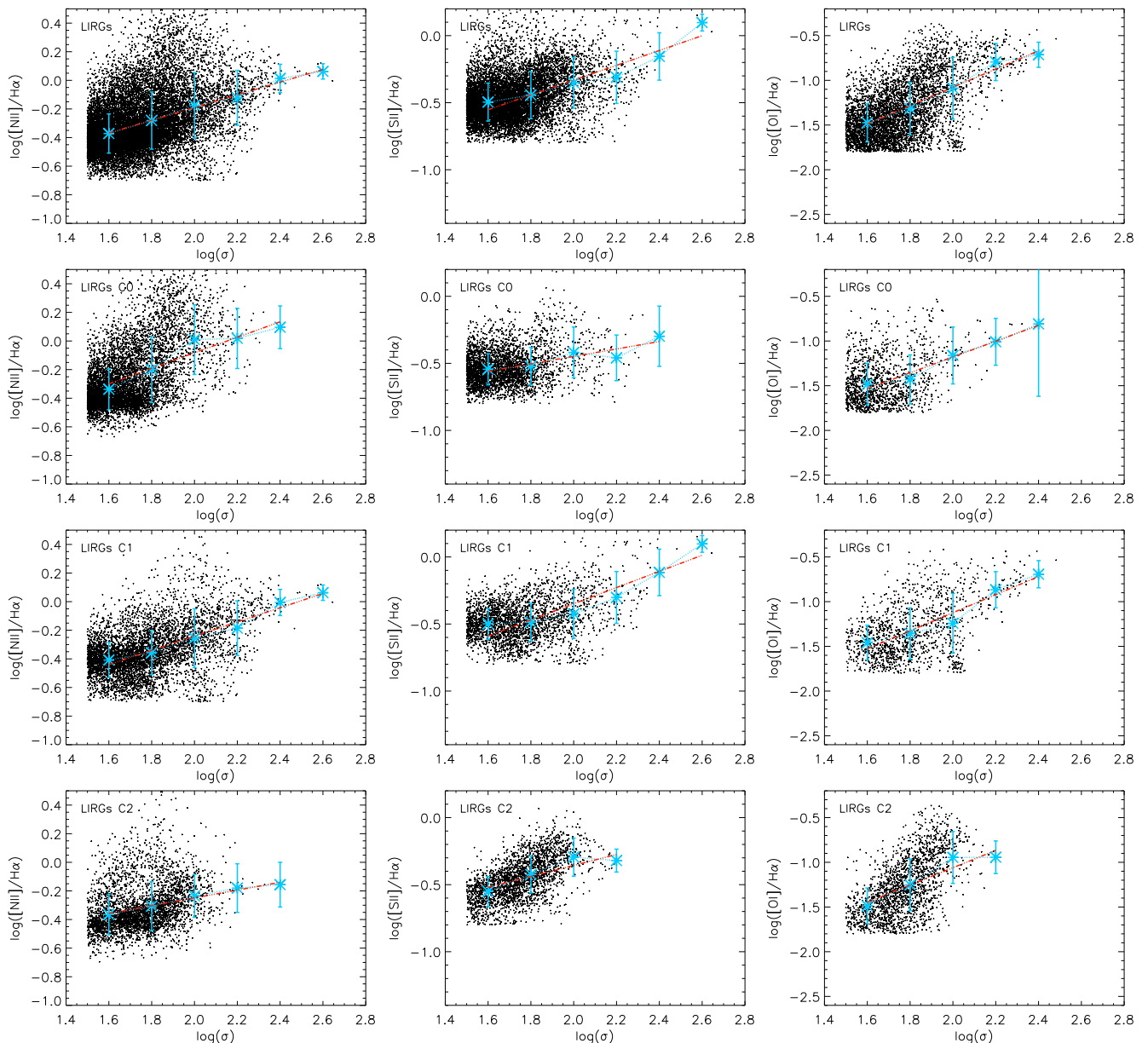


**Fig. 10.** Relation between the velocity dispersion and the  $[\text{N II}]\lambda 6584/\text{H}\alpha$  (left),  $[\text{S II}]\lambda 6717, 6731/\text{H}\alpha$  (middle), and  $[\text{O I}]\lambda 6300/\text{H}\alpha$  (right). Mean and standard deviation of each 0.2 dex bin in the velocity dispersion are shown with blue crosses and error bars respectively. The red dash-3 dotted line in each individual graphic represent the one-degree polynomial fit to these values (see Table 4 for specific values). We refer the reader to the *On-line only* version for the equivalent plots associated with each individual system.

The relations for each individual pointing have been appended in the *On-line only* version (see Fig. 17).

Several conclusions are already evident from these results. Firstly, the ionized gas in the extra-nuclear regions of LIRGs has typically velocity dispersions between  $32 \text{ km s}^{-1}$  (lower limit given by our spectral resolution) and  $125 \text{ km s}^{-1}$ , with very few regions having velocities above this value, independently of the morphology and infrared luminosity.

Secondly, the velocity dispersion of the ionized gas is larger in galaxies with some degree of interaction, i.e. class C1 and C2. While galaxies identified as isolated have a median velocity dispersion of  $37 \text{ km s}^{-1}$ , class C1 and C2 have values of  $46 \text{ km s}^{-1}$  and  $51 \text{ km s}^{-1}$ , respectively. Moreover, the velocity dispersions of class 0 galaxies (i.e. isolated) tend to be concentrated

in the low velocity range, while classes 1 and 2 have a relevant fraction of regions with high velocities. This means that only 5% of the data points for class 0 galaxies present velocity dispersions larger than  $80 \text{ km s}^{-1}$ , while 28% and 16% of those for classes 1 and 2 respectively do when considering, for example, the  $[\text{O I}]\lambda 6300/\text{H}\alpha$  line ratio. These values are much higher than the median velocity dispersions measured in the extranuclear ionized regions of normal galaxies with velocities in the  $20$  to  $30 \text{ km s}^{-1}$  range (Epinat et al. 2010). This is a clear indication that the ionized interstellar medium in LIRGs in general, and even more in interacting LIRGs, is dynamically hotter than the quiescent ISM of normal galaxies due to the strong shocks produced by the tidal forces and by stellar winds in the powerful nuclear starbursts.

Thirdly, there is a clear correlation between the excitation degree and the velocity dispersion in interacting galaxies (class 1) and mergers (class 2), while the evidence of correlation in isolated galaxies (class 0) is poor and restricted to the relation involving the  $[\text{N II}]\lambda 6584/\text{H}\alpha$  line ratio.

To obtain a more quantitative analysis of the degree of the correlation, the linear Pearson correlation coefficient,  $r$ , is used. This coefficient quantifies the degree of correlation between two given quantities that are assumed to follow a linear relation. It varies from  $-1$  to  $+1$ , where  $+1$  ( $-1$ ) means a perfect correlation (anti-correlation) and  $0$  means no-correlation. The Pearson coefficient for the  $\log([\text{S II}]\lambda\lambda 6717, 6731/\text{H}\alpha) - \log(\sigma)$  in the Armus et al. (1989) sample (see also Fig. 8 in Dopita & Sutherland 1995) has a value of  $r = 0.4$ . Hereafter we consider that a positive relation exists between the excitation conditions and velocity dispersion in the ionized gas only if  $r$  is higher than  $0.4$ . The computed  $r$  coefficient for the different groups as well as the polynomial coefficients obtained from a least-square one-degree polynomial fit to the mean of the data in  $0.2$  dex bins in the velocity dispersion appear in Table 4. For the individual pointings, the direct fits to the data are included in the lower right corner of the corresponding panel in Fig. 17 in the *On-line only* version.

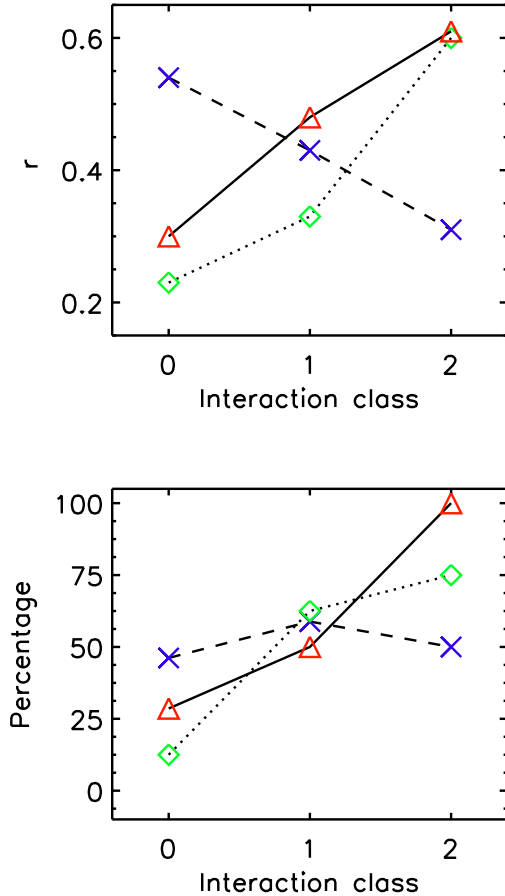


**Fig. 11.** Variation of the  $r$  coefficient (up) and percentage of galaxies with a confidence level higher than 90% showing correlation (down) with the interaction types (0=isolated, 1=interacting pairs, 2=merger remnants) for the three emission line ratios. We used the same line and color code as in Fig. 4 to distinguish among the emission line ratios.

The confidence level of the different relations was estimated by means of the t-Student test. All relations corresponding to the different groups present a confidence level higher than 99.9%. For individual pointings, the  $[\text{N II}]\lambda 6584/\text{H}\alpha - \sigma$  show a larger degree of confidence than those for the  $[\text{S II}]\lambda\lambda 6717, 6731/\text{H}\alpha - \sigma$  and  $[\text{O I}]\lambda 6300/\text{H}\alpha - \sigma$  relations, because the S/N limits the number of points. All relations involving the  $[\text{N II}]\lambda 6584/\text{H}\alpha$  line ratio except the southern member of IRAS 18093–5744 present a level of confidence higher than 95%. For the other line ratios the level of confidence is in general lower. For the  $[\text{S II}]\lambda\lambda 6717, 6731/\text{H}\alpha$  line ratio, 11 out of 36 pointings (i.e. 30%) did not reach a 90% of confidence level. These are IRAS F06295–1735, IRAS F11255–4120, IRAS F11506–3851, IRAS F01159–4443, ESO 297–G012, IC 563, both pointings for IC 564, the northern and central member of IRAS 18093–5744 and IRAS 12596–1529. In the case of the relation involving the  $[\text{O I}]\lambda 6300/\text{H}\alpha$  line ratio 22% of the pointings (i.e. 6 out of 27) did not reach a 90% confidence level. They are the southern member of IRAS F07027–6011, ESO 297–G011, ESO 297–G012, IRAS 08424–3130, the central member of IRAS 18093–5744 and IRAS 12596–1529.

The variation of the Pearson coefficient ( $r$ ) with the interaction class is summarized in the upper part of Fig. 11. The percentage of galaxies in each group showing a correlation coefficient  $r > 0.4$  and a level of confidence higher than 90% is summarized in the lower part of Fig. 11. The quantitative analysis emphasizes the main differences according to the interaction class already mentioned above. The degree of correlation between the excitation properties and the velocity dispersion of the ionized gas when the  $[\text{S II}]\lambda\lambda 6717, 6731/\text{H}\alpha$  and  $[\text{O I}]\lambda 6300/\text{H}\alpha$  line ratios are considered increases with the degree of interaction. In particular, the  $[\text{O I}]\lambda 6300/\text{H}\alpha$  ratio is the best tracer of shocks as already shown in the previous section. When using this ratio, the Pearson correlation coefficient for the class 0 galaxies is  $r = 0.30$ , indicating no correlation. This result supports the idea that shocks are not playing an important role in the ionization of the external areas of this group of LIRGs and agrees well with our previous findings that young stars are the main cause for the ionization. On the other hand, the mean  $r$  values for classes 1 and 2 (0.48 and 0.61, respectively) are well above the 0.4 criterion, which we considered necessary for a good positive relation. This quantitative result clearly supports a direct cause-effect relation between the dynamical status of the gas, i.e. turbulence and shocks traced by the velocity dispersion, and its excitation conditions.

In summary, there are two clear differences between LIRGs classified as class 0 (i.e. isolated), and those classified as class 1 (mostly pairs), and class 2 (mergers). The ionized gas in classes 1 and 2 is characterized by covering a wide range in velocity dispersion with an extension towards higher values than class 0 galaxies. Moreover, the dynamical status of the gas, turbulence and shocks, plays an important role in the excitation of the gas mainly in LIRGs classified as interacting pairs or evolved mergers.

### 3.6. Tidal forces as the origin of shocks in the extra-nuclear regions?

It was shown above that the importance of shocks in large extended regions increases with the interaction class. What is the origin of these shocks? Are the shocks caused by the tidal forces due to the interaction process itself? Or are the shocks produced in stellar superwinds associated with the intense starbursts generated in the nuclear regions?

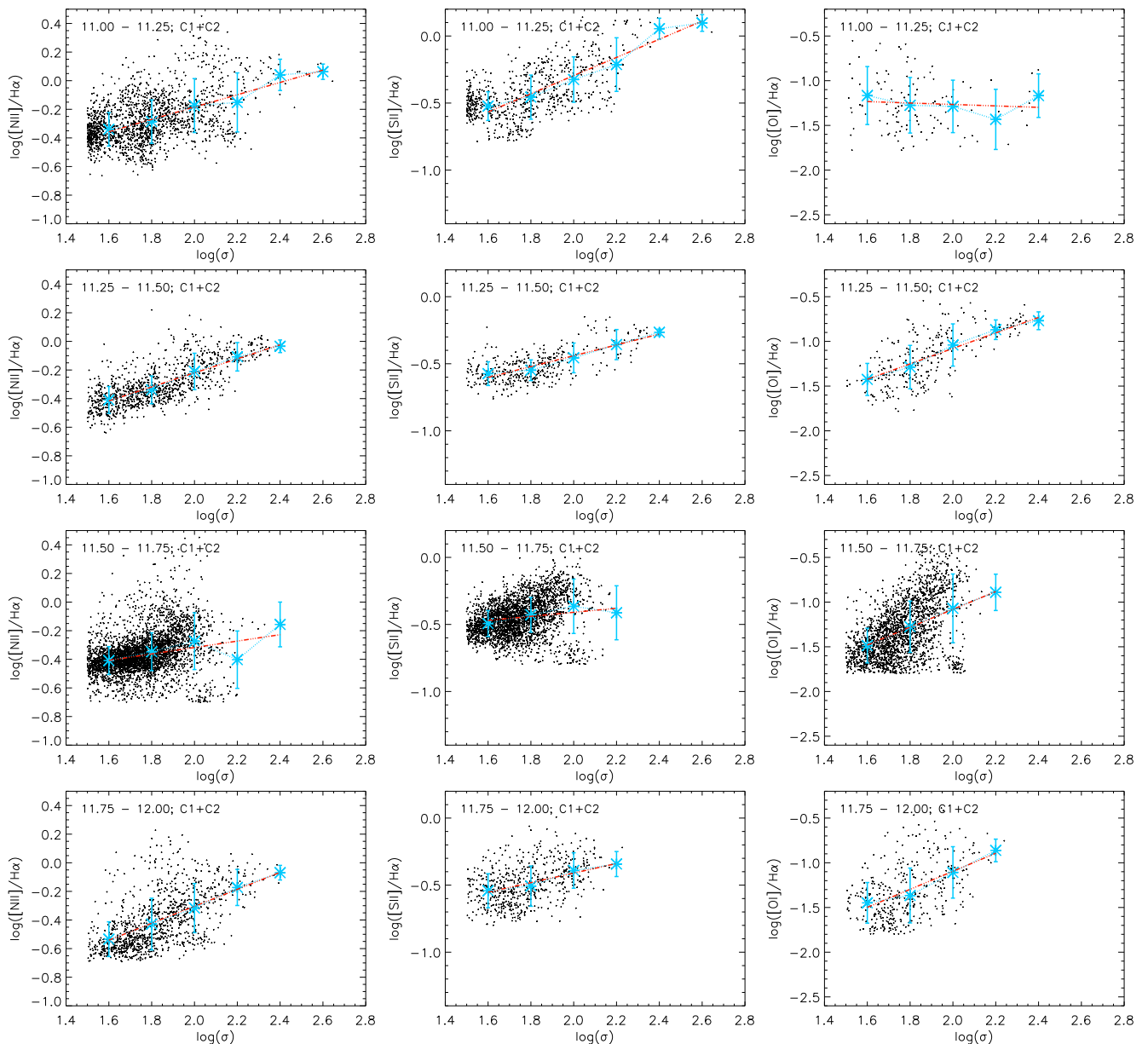


**Fig. 12.** Same as Fig. 10 but for class 1 and 2 systems grouped in four luminosity bins.

To answer these questions, we investigated how the relation between the excitation conditions and gas velocity dispersion varies with the total infrared luminosity of the system. In the sample considered here, only four objects were classified as Seyfert - and thus harboring an AGN- according to their nuclear spectra (Kewley et al. 2001b; Corbett et al. 2003) (see Table 3). Thus the total infrared luminosity is considered in general a direct tracer of the intensity of the star formation, because the infrared luminosity in these galaxies scales linearly with the star-formation rate (e.g. Kennicutt 1998). Figure 12 presents similar relations to those in Fig. 10 for those classes with some degree of interaction (class 1 and 2) but this time binned in four luminosity ranges covering the entire luminosity range of LIRGs (i.e. from  $10^{11}$  to  $10^{12} L_{\odot}$ ).

Contrary to what happens with the interaction class *there is no evidence for a dependence of the correlation coefficient with the luminosity bin*, independently of the utilized line ratio.

Assuming star-formation dominates the energy output in these galaxies (see above), the range in infrared luminosity covered by the sample represents a change of a factor ten in the star-formation rate (see Kennicutt 1984, for the specific relation). Therefore the radiative and mechanical energy released in the surrounding ISM due to supernovae explosions and stellar winds produced in young massive stars would increase linearly with the rate of star formation (see e.g. Colina et al. 1991). These linear relations in the mass, momentum and energy deposition have already been measured in the cool, neutral gas traced by the Na I line (Rupke et al. 2005b). However, these studies do show some evidence for a flattening of these relationships for star-formation rates above  $10 M_{\odot} \text{ yr}^{-1}$  (i.e. LIRG and ULIRG range). It is unclear whether these results would apply to the ionized gas traced by the H $\alpha$  line. The momentum and energy release in the cool, neutral gas is usually a small fraction of the energy in the warm ionized and hot X-ray emitting gas. Moreover, the nonlinear re-

lation between the outflow velocity of the cool gas and the SFR ( $\propto \text{SFR}^{0.35}$ , Martin 2005) could indicate a saturation in the mechanical energy liberated into the more dense neutral gas, but not necessarily in the other phases of the ISM. In addition, the velocity gradients measured in several outflows detected in ULIRGs are inconsistent with the expected gaseous radial flows produced by nuclear (size of 200-300 pc) starbursts (Martin 2006). These gradients could indeed still be consistent with more extended starbursts on scales of kpc, or shocks generated by tidal forces during the interaction process (Martin 2006). Our  $H\alpha$  IFS of (U)LIRGs indicates that the  $H\alpha$  emission is more concentrated than that of the stellar continuum. In particular, the fraction of  $H\alpha$  emission within the central 2 kpc is higher than that of the continuum for about 80% of the cases. However,  $\sim 60\%$  of the objects have more than half of their  $H\alpha$  emission outside the central 2 kpc (see Rodríguez-Zaurín et al. in prep. for details).

Therefore, if the detected evidence of shocks were due to star formation, it would be reasonable to expect a more turbulent gas with stronger outflows and shocks. This could be traced by higher excitation conditions and velocity dispersions in the ionized gas as well as higher correlation degrees. No evidence for any of this is observed in the present data that sample large extra-nuclear regions of several hundreds of pc to several kpc in size, outside the circumnuclear regions.

The comparison between Figs. 10 and 12 indicates that the presence and relevance of shocks are more strongly correlated with the interaction/merging class of a system than with its star formation activity. Indeed, our sample of class 0 galaxies shows on average a level of star formation activity (i.e. infrared luminosity) similar to or slightly lower than that of classes 1 and 2 ( $\log(L/L_{\odot}) = 11.44$  for class 0 against 11.51 and 11.60 for classes 1 and 2, respectively). Note that this statement is valid for our particular sample, which was selected in order to cover all the interaction types and luminosity ranges in a more or less uniform way. However, it does not apply to complete samples of LIRGs, because they show a much higher percentage of interaction/merging systems at higher luminosities (e.g. Sanders & Ishida 2004). These results point to tidal forces associated with the interaction/merging process as the origin for the shock ionization in the extended, extra-nuclear regions. A similar result was found by MAC06, who concluded that the more likely explanation for shocks in five out of the six ULIRGs studied there were tidally induced large scale gas flows caused by the merging process.

Detailed studies of the nearest ULIRG Arp 220 (Colina et al. 2003; McDowell et al. 2003) have also suggested that large extended regions in this system arise purely from merger dynamics and collisional shock heating of the gas. At the same time, footprints associated with starburst superwinds have also been detected (Heckman et al. 1990; Arribas et al. 2001). In Arp 220, the ionized gas plumes that could be associated with superwinds generated in the nuclear starburst form an elongated structure up to a distance of about 2 kpc from the nucleus. However, for the present sample of LIRGs, which show a significant lower star-forming activity based on their  $L_{IR}$  but similar dynamical mass (Hinze & Rieke 2006; Väisänen et al. 2008b,a) and hence similar escape velocity, a smaller area of influence of the stellar superwinds should be expected.

Thus our results indicate that the tidal forces during the interaction process are the mechanism producing the ionizing shocks in the extended extra-nuclear regions in LIRGs. This is still compatible with the existence of SGWs produced in nuclear starbursts at distances closer to the nucleus (i.e. radius of 1 to 2

kpc), or AGN ionizing cones along particular orientations (e.g. Arp 299, García-Marín et al. 2006).

### 3.7. Interacting LIRGs and ULIRGs. Towards a common $\log([\text{O I}]\lambda 6300/H\alpha) - \log(\sigma)$ relation?

In previous sections we showed that our IFS data indicate that shocks produced by the tidal forces in interacting and merging LIRGs play a relevant role in the excitation of the extended ionized regions, without any clear relation with the intensity of the star formation. Because ULIRGs are the extreme cases of interactions and mergers, one may wonder how the LIRGs situation compares with that for the ULIRGs. For that purpose, we compared our results with those presented in MAC06. The relatively small sample of MAC06 (i.e. six ULIRGs systems, nine galaxies) was made out of three class 1 systems (IRAS 08572+3915, IRAS 12112+0305, IRAS 14348-1447) and three class 2 systems (IRAS 15206+3342, IRAS 15250+3609, IRAS 17208-0014). We found that in all the systems but IRAS 17208-0014 the extra-nuclear extended regions were well explained by ionization due to fast shocks with velocities of  $150 - 500 \text{ km s}^{-1}$ . Because none of the systems in the MAC06's ULIRGs sample is classified as isolated (class 0), we present in Fig. 13 (second row) the line ratio vs. velocity dispersion only for LIRGs of classes 1 and 2.

Considering the best shock tracer, the  $[\text{O I}]\lambda 6300/H\alpha$  line ratio, the similarity of the  $\log([\text{O I}]\lambda 6300/H\alpha) - \log(\sigma)$  correlation found independently for LIRGs and ULIRGs is remarkable. Because the average infrared luminosity ( $\log(L_{ir}/L_{\odot})$ ) of the ULIRG sample is 12.24, this extends the previous result found for class 1 and class 2 LIRGs, where a similar linear relation exists for the entire LIRG luminosity range, independent of the luminosity beam selected. Although the number of ULIRGs in the MAC06 sample is small, the combined results suggest a common relation between the excitation and dynamical properties of the ionized gas in interacting and merging (U)LIRGs over the entire infrared luminosity range of  $\log(L_{ir}/L_{\odot}) = 11.1 - 12.3$  covered by these two samples. This relation is best traced by the direct proportionality (slope of  $\sim 1.0$ ) between  $\log([\text{O I}]\lambda 6300/H\alpha)$  and  $\log(\sigma)$  (see Tables 4 and 6 for the specific slopes). A larger sample of about 20 ULIRGs with available optical integral field spectroscopy is currently studied (García-Marín et al. in preparation) to further investigate the reality of the relation for both LIRGs and ULIRGs and its physical interpretation.

## 4. Conclusions

The two-dimensional ionization structure of the extended (few to several kpc) ionized gas in a representative sample of 32 low- $z$  LIRGs (i.e.  $\log(L_{ir}/L_{\odot}) = 11.00 - 12.00$  luminosity range) was investigated with the VIMOS integral field spectrograph. The sample covers isolated galaxies, as well as interacting galaxies and systems in an advanced stage of the merger. This paper investigates the nature and origin of the main ionization mechanisms operating in the extra-nuclear regions of these systems based on several thousands of independent measurements of the emission line ratios (up to twenty 24 000 for  $[\text{N II}]\lambda 6584/H\alpha$ ) and velocity dispersions.

The present study is part of a larger project devoted to the study of the two-dimensional structure for the stars and ionized gas as well as its kinematics and ionization conditions in representative samples of LIRGs and ULIRGs using optical IFS. The main results of this study can be summarized as follows:

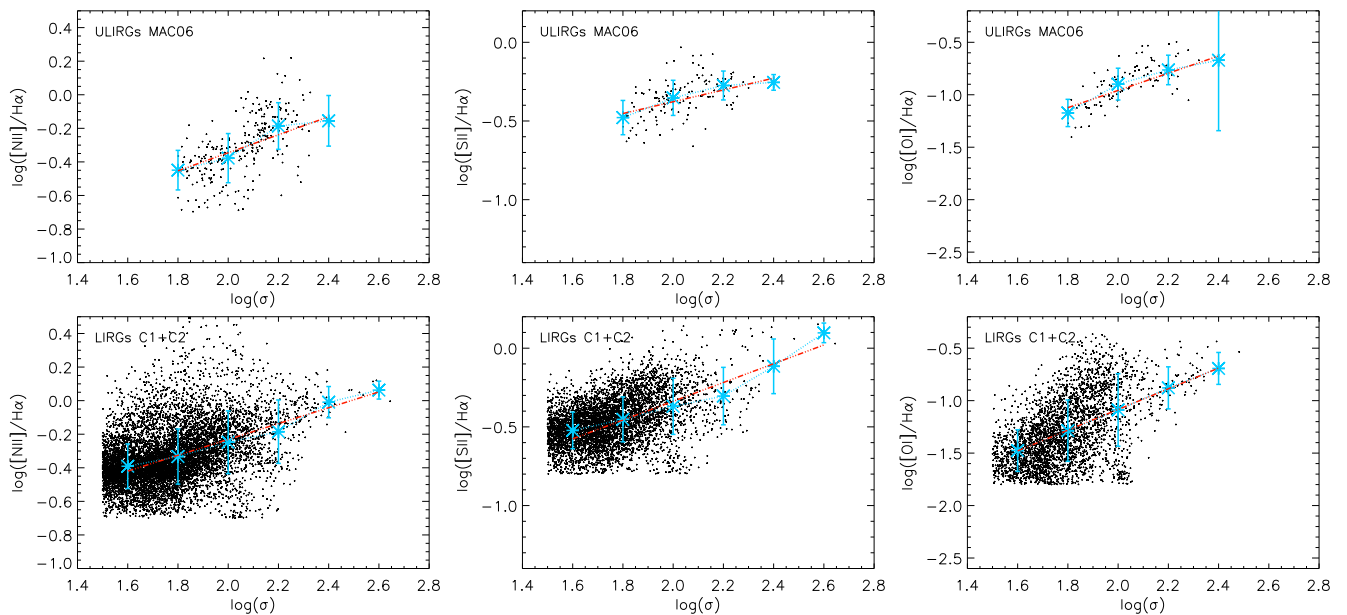


**Fig. 13.** *Upper row:* Same as Fig. 10, but for all systems in MAC06 but IRAS 17208–0014. This is similar to the first row of Fig. 4 of MAC06 but we plotted the same ranges in the axes as in Fig. 10 for a better comparison with the results in the present paper. *Lower row:* Same as Fig. 10 for the combined class 1 + class 2 group.

1. The distribution of the  $[\text{N II}]\lambda 6584/\text{H}\alpha$  line ratio does not show any significant variations with the interaction class, with most regions presenting a ratio typical of  $\text{H II}$  regions. The  $[\text{S II}]\lambda\lambda 6717, 6731/\text{H}\alpha$  and  $[\text{O I}]\lambda 6300/\text{H}\alpha$  line ratios do however show a change in their distribution with an extension towards higher excitation (i.e. LINER-like excitation) for galaxies classified as interacting pairs and advanced mergers. This change is more pronounced for the  $[\text{O I}]\lambda 6300/\text{H}\alpha$  ratio.

2. There is an anti-correlation between the ionization degree and the  $\text{H}\alpha$  surface brightness independently of the interaction type and similar to what occurs in our Galaxy or in the so-called DIG in other spiral galaxies. Most of the observed line ratios are similar to those found in  $\text{H II}$  regions in our Galaxy, but there is a relatively large percentage of line ratios similar to those for DIGs.

3. The nature of the ionization sources was investigated comparing the measured  $[\text{S II}]\lambda\lambda 6717, 6731/\text{H}\alpha$  vs.  $[\text{N II}]\lambda 6584/\text{H}\alpha$  and  $[\text{O I}]\lambda 6300/\text{H}\alpha$  vs.  $[\text{N II}]\lambda 6584/\text{H}\alpha$  line ratios with the predictions of ionization due to stars ( $\text{H II}$  regions), TML, shocks (DIGs) and power-law (AGN) spectra. Turbulent Mixing Layers do not seem to play a major role in the ionization of the extranuclear regions. Line ratios in LIRGs classified as isolated can mostly be explained as caused by ionization due to young stars. On the other hand, the ionization in a large fraction of the regions in systems with some degree of interaction cannot be due to stars but is better explained by high velocity shocks. This is particularly evident when using the best shock tracer, i.e. the  $[\text{O I}]\lambda 6300/\text{H}\alpha$  vs.  $[\text{N II}]\lambda 6584/\text{H}\alpha$  diagram. Independently of the ionization mechanisms, only models with metallicity between solar and twice solar are able to explain the observed line ratios.

4. Local velocity dispersions increase with the interaction degree, with medians of 37, 46, and 51  $\text{km s}^{-1}$  for class 0, 1, and 2 respectively, and are higher than those typically found in normal spirals ( $\sim 20 - 30 \text{ km s}^{-1}$ , Epinat et al. 2010). This indicates that the ionized ISM in LIRGs is dynamically hotter than

the quiescent ISM of normal galaxies due to strong shocks produced by tidal forces and stellar winds associated to the nuclear starburst.

5. There is a positive relation between the degree of excitation (as traced by the emission line ratios) and the velocity dispersion of the ionized gas in LIRGs classified as interacting systems, and mergers, while this relation is not observed in isolated systems. This relation is better seen when using the  $[\text{O I}]\lambda 6300/\text{H}\alpha$  and  $[\text{S II}]\lambda\lambda 6717, 6731/\text{H}\alpha$  line ratios, and supports the scenario where the relevance of shocks as ionizing sources in the extranuclear extended regions of LIRGs increases when there is some degree of interaction.

6. The relation between the degree of excitation and the velocity dispersion of the ionized gas in interacting and merging LIRGs does not clearly improve with the infrared luminosity (i.e. star formation rate) of the systems. Thus the interaction process itself rather than superwinds caused by the star formation seems to be the main origin of the shocks in the extended extra-nuclear regions, assuming that the release of energy into the ISM is proportional to the SFR. This result is still compatible with stellar superwinds in the internal regions of these systems, and/or along certain preferential directions associated with AGN-related outflows.

7. A comparison between the sub-sample of interacting/merging LIRGs and a small sample of ULIRGs suggests the existence of a common positive  $\log([\text{O I}]\lambda 6300/\text{H}\alpha) - \log(\sigma)$  relation. If confirmed, these results will provide further evidence for the tidal origin of shocks in these galaxies over the entire LIRG and ULIRG luminosity range. A study with a larger sample of ULIRGs is under way to confirm the result.

*Acknowledgements.* We thank J. Alfonso-Garzón for her help in the initial stages of this project. We also thank the anonymous referee for his/her careful and detailed review of the manuscript that helped to greatly improve this paper. Based on observations collected at the European Organisation for Astronomical Research in the Southern Hemisphere, Chile (ESO Programs 076.B-0479(A), 078.B-0072(A) and 081.B-0108(A)). AM-I is grateful for the hospitality of the Instituto de Estructura de la Materia where part of this work was performed. This

paper uses the plotting package `jmaplot`, developed by Jesús Maíz-Apellániz, <http://dae45.iaa.csic.es:8080/~jmaiz/software>. This research made use of the NASA/IPAC Extragalactic Database (NED), which is operated by the Jet Propulsion Laboratory, California Institute of Technology, under contract with the National Aeronautics and Space Administration.

This work has been supported by the Spanish Ministry for Education and Science under grants PNE2005-01480 and ESP2007-65475-C02-01. AM-I is supported by the Spanish Ministry of Science and Innovation (MICINN) under the program "Specialization in International Organisms", ref. ES2006-0003. MG-M is supported by the German federal department for education and research (BMBF) under the project numbers: 50OS0502 & 50OS0801.

## References

- Allen, M. G., Groves, B. A., Dopita, M. A., Sutherland, R. S., & Kewley, L. J. 2008, *ApJS*, 178, 20
- Alonso-Herrero, A., García-Marín, M., Monreal-Ibero, A., et al. 2009, *A&A*, 506, 1541
- Alonso-Herrero, A., García-Marín, M., Rodríguez-Zaurín, J., et al. 2010, submitted
- Alonso-Herrero, A., Rieke, G. H., Rieke, M. J., et al. 2006, *ApJ*, 650, 835
- Alonso-Herrero, A., Rieke, G. H., Rieke, M. J., & Scoville, N. Z. 2002, *AJ*, 124, 166
- Armus, L., Heckman, T. M., & Miley, G. K. 1989, *ApJ*, 347, 727
- Arribas, S., Bushouse, H., Lucas, R. A., Colina, L., & Borne, K. D. 2004, *AJ*, 127, 2522
- Arribas, S., Carter, D., Cavaller, L., et al. 1998, in *Society of Photo-Optical Instrumentation Engineers (SPIE) Conference Series*, Vol. 3355, *Society of Photo-Optical Instrumentation Engineers (SPIE) Conference Series*, ed. S. D'Odorico, 821–827
- Arribas, S., Colina, L., & Clements, D. 2001, *ApJ*, 560, 160
- Arribas, S., Colina, L., Monreal-Ibero, A., et al. 2008, *A&A*, 479, 687
- Asplund, M., Grevesse, N., Sauval, A. J., Allende Prieto, C., & Kiselman, D. 2004, *A&A*, 417, 751
- Baldwin, J. A., Phillips, M. M., & Terlevich, R. 1981, *PASP*, 93, 5
- Bedregal, A. G., Colina, L., Alonso-Herrero, A., & Arribas, S. 2009, *ApJ*, 698, 1852
- Bingham, R. G., Gellatly, D. W., Jenkins, C. R., & Worswick, S. P. 1994, in *Society of Photo-Optical Instrumentation Engineers (SPIE) Conference Series*, Vol. 2198, *Society of Photo-Optical Instrumentation Engineers (SPIE) Conference Series*, ed. D. L. Crawford & E. R. Craine, 56–64
- Blanc, G. A., Heiderman, A., Gebhardt, K., Evans, N. J., & Adams, J. 2009, *ApJ*, 704, 842
- Borne, K. D., Bushouse, H., Lucas, R. A., & Colina, L. 2000, *ApJ*, 529, L77
- Bushouse, H. A., Borne, K. D., Colina, L., et al. 2002, *ApJS*, 138, 1
- Clements, D. L., Sutherland, W. J., McMahon, R. G., & Saunders, W. 1996, *MNRAS*, 279, 477
- Colina, L., Arribas, S., & Monreal-Ibero, A. 2005, *ApJ*, 621, 725
- Colina, L., González Delgado, R., Mas-Hesse, J. M., Leitherer, C., & Jiménez Bailón, E. 2003, *ApJ*, 582, 1269
- Colina, L., Lipari, S., & Macchetto, F. 1991, *ApJ*, 379, 113
- Collins, J. A. & Rand, R. J. 2001, *ApJ*, 551, 57
- Corbett, E. A., Kewley, L., Appleton, P. N., et al. 2003, *ApJ*, 583, 670
- Cui, J., Xia, X.-Y., Deng, Z.-G., Mao, S., & Zou, Z.-L. 2001, *AJ*, 122, 63
- Dopita, M. A., Fischera, J., Sutherland, R. S., et al. 2006, *ApJS*, 167, 177
- Dopita, M. A. & Sutherland, R. S. 1995, *ApJ*, 455, 468
- Eisenhauer, F., Abuter, R., Bickert, K., et al. 2003, in *Society of Photo-Optical Instrumentation Engineers (SPIE) Conference Series*, Vol. 4841, *Society of Photo-Optical Instrumentation Engineers (SPIE) Conference Series*, ed. M. Iye & A. F. M. Moorwood, 1548–1561
- Elbaz, D., Cesarsky, C. J., Chaniol, P., et al. 2002, *A&A*, 384, 848
- Epinat, B., Amram, P., Balkowski, C., & Marcelin, M. 2010, *MNRAS*, 401, 2113
- Evans, A. S., Mazzarella, J. M., Surace, J. A., & Sanders, D. B. 2002, *ApJ*, 580, 749
- Farrah, D., Bernard-Salas, J., Spoon, H. W. W., et al. 2007, *ApJ*, 667, 149
- García-Marín, M., Colina, L., Arribas, S., Alonso-Herrero, A., & Mediavilla, E. 2006, *ApJ*, 650, 850
- García-Marín, M., Colina, L., Arribas, S., & Monreal-Ibero, A. 2009, *A&A*, 505, 1319
- Genzel, R., Lutz, D., Sturm, E., et al. 1998, *ApJ*, 498, 579
- Groves, B. A., Dopita, M. A., & Sutherland, R. S. 2004, *ApJS*, 153, 75
- Heckman, T. M., Armus, L., & Miley, G. K. 1990, *ApJS*, 74, 833
- Heckman, T. M., Lehnert, M. D., Strickland, D. K., & Armus, L. 2000, *ApJS*, 129, 493
- Hinz, J. L. & Rieke, G. H. 2006, *ApJ*, 646, 872
- Kauffmann, G., Heckman, T. M., Tremonti, C., et al. 2003, *MNRAS*, 346, 1055
- Kennicutt, Jr., R. C. 1984, *ApJ*, 287, 116
- Kennicutt, Jr., R. C. 1998, *ARA&A*, 36, 189
- Kewley, L. J., Dopita, M. A., Sutherland, R. S., Heisler, C. A., & Trevena, J. 2001a, *ApJ*, 556, 121
- Kewley, L. J., Groves, B., Kauffmann, G., & Heckman, T. 2006, *MNRAS*, 372, 961
- Kewley, L. J., Heisler, C. A., Dopita, M. A., & Lumsden, S. 2001b, *ApJS*, 132, 37
- Kim, D.-C., Sanders, D. B., Veilleux, S., Mazzarella, J. M., & Soifer, B. T. 1995, *ApJS*, 98, 129
- Le Floc'h, E., Papovich, C., Dole, H., et al. 2005, *ApJ*, 632, 169
- LeFèvre, O., Saisse, M., Mancini, D., et al. 2003, in *Society of Photo-Optical Instrumentation Engineers (SPIE) Conference Series*, Vol. 4841, *Society of Photo-Optical Instrumentation Engineers (SPIE) Conference Series*, ed. M. Iye & A. F. M. Moorwood, 1670–1681
- Lehnert, M. D. & Heckman, T. M. 1996, *ApJ*, 462, 651
- Leitherer, C., Schaerer, D., Goldader, J. D., et al. 1999, *ApJS*, 123, 3
- Lonsdale, C. J., Farrah, D., & Smith, H. E. 2006, *Ultraluminous Infrared Galaxies*, ed. J. W. Mason (Springer Verlag), 285–+
- Madsen, G. J., Reynolds, R. J., & Haffner, L. M. 2006, *ApJ*, 652, 401
- Martin, C. L. 2005, *ApJ*, 621, 227
- Martin, C. L. 2006, *ApJ*, 647, 222
- Mathis, J. S. 2000, *ApJ*, 544, 347
- McDowell, J. C., Clements, D. L., Lamb, S. A., et al. 2003, *ApJ*, 591, 154
- Mihos, J. C. & Hernquist, L. 1996, *ApJ*, 464, 641
- Miller, S. T. & Veilleux, S. 2003, *ApJ*, 592, 79
- Monreal-Ibero, A., Arribas, S., & Colina, L. 2006, *ApJ*, 637, 138
- Moshir, M. & et al. 1990, in *IRAS Faint Source Catalogue*, version 2.0 (1990), 0–+
- Naab, T., Jesseit, R., & Burkert, A. 2006, *MNRAS*, 372, 839
- Nardini, E., Risaliti, G., Salvati, M., et al. 2008, *MNRAS*, 385, L130
- Pérez-González, P. G., Rieke, G. H., Egami, E., et al. 2005, *ApJ*, 630, 82
- Reynolds, R. J., Haffner, L. M., & Tufte, S. L. 1999, *ApJ*, 525, L21
- Risaliti, G., Maiolino, R., Marconi, A., et al. 2006, *MNRAS*, 365, 303
- Rodríguez-Zaurín, J., Arribas, S., Monreal-Ibero, A., et al. 2010, in prep.
- Roth, M. M., Kelz, A., Fechner, T., et al. 2005, *PASP*, 117, 620
- Rupke, D. S., Veilleux, S., & Sanders, D. B. 2002, *ApJ*, 570, 588
- Rupke, D. S., Veilleux, S., & Sanders, D. B. 2005a, *ApJS*, 160, 87
- Rupke, D. S., Veilleux, S., & Sanders, D. B. 2005b, *ApJS*, 160, 115
- Rupke, D. S. N., Veilleux, S., & Baker, A. J. 2008, *ApJ*, 674, 172
- Sanders, D. & Ishida, C. 2004, in *Astronomical Society of the Pacific Conference Series*, Vol. 320, *The Neutral ISM in Starburst Galaxies*, ed. S. Aalto, S. Huttemeister, & A. Pedlar, 230–+
- Sanders, D. B., Mazzarella, J. M., Kim, D.-C., Surace, J. A., & Soifer, B. T. 2003, *AJ*, 126, 1607
- Sanders, D. B. & Mirabel, I. F. 1996, *ARA&A*, 34, 749
- Scoville, N. Z., Evans, A. S., Thompson, R., et al. 2000, *AJ*, 119, 991
- Slavin, J. D., Shull, J. M., & Begelman, M. C. 1993, *ApJ*, 407, 83
- Stasińska, G., Cid Fernandes, R., Mateus, A., Sodré, L., & Asari, N. V. 2006, *MNRAS*, 371, 972
- Tremonti, C. A., Heckman, T. M., Kauffmann, G., et al. 2004, *ApJ*, 613, 898
- Väisänen, P., Mattila, S., Kniazev, A., et al. 2008a, *MNRAS*, 384, 886
- Väisänen, P., Ryder, S., Mattila, S., & Kotilainen, J. 2008b, *ApJ*, 689, L37
- Veilleux, S., Kim, D.-C., & Sanders, D. B. 1999, *ApJ*, 522, 113
- Veilleux, S., Kim, D.-C., & Sanders, D. B. 2002, *ApJS*, 143, 315
- Veilleux, S., Kim, D.-C., Sanders, D. B., Mazzarella, J. M., & Soifer, B. T. 1995, *ApJS*, 98, 171
- Veilleux, S. & Osterbrock, D. E. 1987, *ApJS*, 63, 295
- York, D. G., Adelman, J., Anderson, Jr., J. E., et al. 2000, *AJ*, 120, 1579
- Yuan, T.-T., Kewley, L. J., & Sanders, D. B. 2010, *MNRAS*, 709, 884

**Table 1.** VIMOS LIRG sample: For each pointing, the total number of data points, mean value and standard deviation for the different line ratios and velocity dispersion are given.

Galaxy (IRAS number)	$\log L_{ir}^{(1)}$ ( $L_{\odot}$ )	D (Mpc)	Scale (pc'')	[N II] $\lambda$ 6584/H $\alpha$		[S II] $\lambda$ \lambda6717,6731/H $\alpha$		[O I] $\lambda$ 6300/H $\alpha$		$\sigma^{(2)}$ (km s $^{-1}$ )	
				n	$\bar{x} \pm \sigma(x)$	n	$\bar{x} \pm \sigma(x)$	n	$\bar{x} \pm \sigma(x)$	n	$\bar{x} \pm \sigma(x)$
Class 0											
F06295–1735	11.27	92.7	431	998	0.38 $\pm$ 0.07	486	0.31 $\pm$ 0.06	194	0.05 $\pm$ 0.04	1118	33 $\pm$ 11
F06592–6313	11.91	100.0	464	199	0.82 $\pm$ 0.32	...	...	...	...	266	54 $\pm$ 33
F07027–6011 N	11.64	137.4	626	342	0.40 $\pm$ 0.09	94	0.30 $\pm$ 0.06	92	0.07 $\pm$ 0.04	387	32 $\pm$ 11
F07027–6011 S		137.4	626	163	0.61 $\pm$ 0.17	74	0.24 $\pm$ 0.05	49	0.03 $\pm$ 0.02	177	72 $\pm$ 17
F07160–6215	11.16	46.7	221	755	0.92 $\pm$ 0.61	189	0.33 $\pm$ 0.16	...	...	888	69 $\pm$ 37
F10015–0614	11.77	73.1	343	1298	0.41 $\pm$ 0.10	850	0.31 $\pm$ 0.08	137	0.03 $\pm$ 0.01	1312	51 $\pm$ 13
F10409–4556	11.26	91.4	425	928	0.49 $\pm$ 0.25	...	...	...	...	1083	39 $\pm$ 16
F10567–4310	11.07	74.6	350	1154	0.44 $\pm$ 0.15	270	0.25 $\pm$ 0.06	...	...	1153	29 $\pm$ 11
F11255–4120	11.04	70.9	333	759	0.58 $\pm$ 0.28	173	0.28 $\pm$ 0.06	...	...	782	33 $\pm$ 20
F11506–3851	11.30	46.6	221	887	0.67 $\pm$ 0.23	434	0.33 $\pm$ 0.13	327	0.04 $\pm$ 0.03	914	41 $\pm$ 14
F12115–4656	11.11	80.3	375	724	0.52 $\pm$ 0.18	462	0.31 $\pm$ 0.08	274	0.03 $\pm$ 0.02	847	41 $\pm$ 12
F13229–2934	11.29	59.3	280	865	1.21 $\pm$ 0.71	295	0.42 $\pm$ 0.19	146	0.07 $\pm$ 0.06	932	65 $\pm$ 24
F22132–3705	11.22	49.3	234	1706	0.41 $\pm$ 0.08	1490	0.29 $\pm$ 0.08	712	0.03 $\pm$ 0.02	1714	32 $\pm$ 8
Class 1											
F01159–4443	11.48	99.8	462	558	0.45 $\pm$ 0.12	170	0.29 $\pm$ 0.06	97	0.07 $\pm$ 0.05	646	48 $\pm$ 20
ESO 297-G011	11.18	75.0	352	1339	0.45 $\pm$ 0.11	627	0.32 $\pm$ 0.08	109	0.03 $\pm$ 0.03	1404	32 $\pm$ 10
ESO 297-G012		75.0	352	223	0.54 $\pm$ 0.15	97	0.38 $\pm$ 0.10	80	0.10 $\pm$ 0.08	226	91 $\pm$ 31
F06076–2139	11.67	165.0	743	274	0.63 $\pm$ 0.45	...	...	...	...	313	40 $\pm$ 25
F06259–4708 P1	11.91	171.1	769	443	0.48 $\pm$ 0.24	221	0.27 $\pm$ 0.10	149	0.04 $\pm$ 0.04	550	81 $\pm$ 40
F06259–4708 P2		171.1	769	279	0.30 $\pm$ 0.08	201	0.36 $\pm$ 0.11	163	0.06 $\pm$ 0.05	404	59 $\pm$ 20
08424–3130	11.04	70.1	329	241	0.80 $\pm$ 0.47	108	0.38 $\pm$ 0.15	56	0.05 $\pm$ 0.03	392	73 $\pm$ 32
F08520–6850	11.83	205.4	909	196	0.34 $\pm$ 0.10	103	0.39 $\pm$ 0.10	39	0.05 $\pm$ 0.03	318	72 $\pm$ 31
IC563 <sup>(3,4)</sup>	11.21	89.0	415	873	0.36 $\pm$ 0.08	491	0.33 $\pm$ 0.10	264	0.04 $\pm$ 0.02	1007	38 $\pm$ 9
IC564 P1 <sup>(3,4)</sup>		89.0	415	727	0.42 $\pm$ 0.12	163	0.35 $\pm$ 0.12	...	...	843	33 $\pm$ 10
IC564 P2 <sup>(3,4)</sup>		89.0	415	495	0.37 $\pm$ 0.08	77	0.27 $\pm$ 0.09	...	...	635	36 $\pm$ 14
12042–3140	11.37	101.1	468	540	0.58 $\pm$ 0.23	246	0.33 $\pm$ 0.13	176	0.08 $\pm$ 0.06	611	85 $\pm$ 46
12596–1529	11.07	69.0	324	433	0.42 $\pm$ 0.13	226	0.41 $\pm$ 0.14	35	0.03 $\pm$ 0.02	487	64 $\pm$ 34
F14544–4255 E	11.11	68.2	320	322	0.45 $\pm$ 0.19	53	0.21 $\pm$ 0.06	...	...	370	55 $\pm$ 15
F14544–4255 W		68.2	320	356	0.70 $\pm$ 0.26	165	0.68 $\pm$ 0.27	87	0.15 $\pm$ 0.09	392	66 $\pm$ 24
18093–5744 N	11.57	75.3	353	804	0.41 $\pm$ 0.12	528	0.36 $\pm$ 0.09	105	0.03 $\pm$ 0.02	886	46 $\pm$ 13
18093–5744 C		75.3	353	373	0.23 $\pm$ 0.07	204	0.23 $\pm$ 0.11	61	0.02 $\pm$ 0.01	634	80 $\pm$ 35
18093–5744 S		75.3	353	316	0.46 $\pm$ 0.10	185	0.33 $\pm$ 0.06	28	0.03 $\pm$ 0.02	359	47 $\pm$ 16
Class 2											
F04315–0840	11.69	69.1	325	763	0.58 $\pm$ 0.24	398	0.42 $\pm$ 0.13	407	0.10 $\pm$ 0.08	759	66 $\pm$ 32
08355–4944	11.60	113.1	521	260	0.32 $\pm$ 0.07	121	0.25 $\pm$ 0.06	108	0.03 $\pm$ 0.02	347	59 $\pm$ 20
F10038–3338	11.77	149.9	679	172	0.60 $\pm$ 0.29	58	0.44 $\pm$ 0.18	42	0.13 $\pm$ 0.09	303	55 $\pm$ 28
10257–4338	11.69	40.4	192	1698	0.45 $\pm$ 0.11	1573	0.39 $\pm$ 0.13	1403	0.06 $\pm$ 0.05	1744	61 $\pm$ 19
12116–5615 <sup>(3)</sup>	11.61	80.3	375	90	0.84 $\pm$ 0.29	33	0.34 $\pm$ 0.13	...	...	114	70 $\pm$ 15
13001–2339 <sup>(3)</sup>	11.48	94.5	439	320	0.78 $\pm$ 0.28	80	0.63 $\pm$ 0.16	96	0.21 $\pm$ 0.07	388	117 $\pm$ 54
17138–1017 <sup>(3)</sup>	11.41	75.2	352	235	0.53 $\pm$ 0.15	87	0.38 $\pm$ 0.10	...	...	257	63 $\pm$ 18
21453–3511	11.41	70.0	329	1112	0.61 $\pm$ 0.41	476	0.23 $\pm$ 0.11	63	0.04 $\pm$ 0.05	1136	43 $\pm$ 19

<sup>(1)</sup> Logarithm of the infrared luminosity,  $L_{ir} = L(8 - 1000\mu\text{m})$ , in units of solar bolometric luminosity, calculated using the fluxed in the four IRAS bands as given in Sanders et al. (2003), when available. Otherwise from the IRAS fluxes given in IRAS Point Source and Faint Source catalogs Moshir & et al. (1990). When a system of more than one galaxy is observed using several VIMOS pointings, the infrared luminosity of the entire system is indicated in the data corresponding to the first galaxy of the system.

<sup>(2)</sup> Velocity dispersion derived from the H $\alpha$  line.

<sup>(3)</sup> Classification uncertain. Not used in the analysis of systems grouped by interaction class.

<sup>(4)</sup> Members of IRAS 09437+0317.

**Table 2.** Median, standard deviation, and number of data points for the distributions of the different groups and line ratios.

Group	$\log([\text{N II}]\lambda 6584/\text{H}\alpha)$			$\log([\text{S II}]\lambda\lambda 6717,6731/\text{H}\alpha)$			$\log([\text{O I}]\lambda 6300/\text{H}\alpha)$		
	Median	Std Dev	N	Median	Std Dev	N	Median	Std Dev	N
All	-0.37	0.18	24 017	-0.49	0.16	12 564	-1.46	0.34	5 733
Class 0	-0.37	0.18	10 605	-0.55	0.13	4 932	-1.56	0.28	1 953
Class 1	-0.38	0.17	6 680	-0.49	0.18	3 140	-1.43	0.33	1 349
Class 2	-0.36	0.16	3 992	-0.48	0.17	2 628	-1.35	0.35	2 023

**Table 3.** Ionization in the extra-nuclear ionized regions of LIRGs.

Galaxy (IRAS number)	Mechanism <sup>(a)</sup>	$r$ <sup>(b)</sup>	Comment
Class 0			
F06295–1735	Young stars	0.22	
F06592–6313	...	0.42	No [O I] $\lambda$ 6300 nor [S II] $\lambda$ 6717,6731 data. $r$ based on [N II] $\lambda$ 6584/H $\alpha$ .
F07027–6011 N <sup>(c)</sup>	Young stars and shocks (100-200 km s <sup>-1</sup> )	0.44	Part of the shocks may be associated to the nucleus according [O I] $\lambda$ 6300/H $\alpha$ map.
F07027–6011 S	Young stars	0.21	$r$ based on [S II] $\lambda$ 6717,6731/H $\alpha$ . $r$ based on [O I] $\lambda$ 6300/H $\alpha$ not reliable.
F07160–6215	Shocks (100-300 km s <sup>-1</sup> )	0.31	$r$ based on [S II] $\lambda$ 6717,6731/H $\alpha$ . No [O I] $\lambda$ 6300 data.
F10015–0614	Young stars	0.15	
F10409–4556	...	0.37	$r$ based on [N II] $\lambda$ 6584/H $\alpha$ . No [O I] $\lambda$ 6300 nor [S II] $\lambda$ 6717,6731 data.
F10567–4310	Young stars	0.23	$r$ based on [S II] $\lambda$ 6717,6731/H $\alpha$ . No [O I] $\lambda$ 6300 data.
F11254–4120	Young stars	0.71	$r$ based on [N II] $\lambda$ 6584/H $\alpha$ . $r$ based on [S II] $\lambda$ 6717,6731/H $\alpha$ not reliable. No [O I] $\lambda$ 6300 data. Possible shocks associated to the bar according to the [S II] $\lambda$ 6717,6731/H $\alpha$ map.
F11506–3851	Young stars	0.19	Some small areas better explained with low velocity shocks.
F12115–4656	Young stars	-0.24	
F13229–2934 <sup>(d)</sup>	Shocks (100-300 km s <sup>-1</sup> )	0.47	Some areas explained by stars, mostly associated with the arms. Part of the high excitation may be associated to the nucleus according to the [O I] $\lambda$ 6300/H $\alpha$ map. Small areas better explained with low velocity (<100 km s <sup>-1</sup> ) shocks.
F22132–3705	Young stars	0.10	
Class 1			
F01159–4443	Low velocity (<100 km s <sup>-1</sup> ) shocks	0.23	Some regions explained by stars.
ESO 297-G011	Young stars	-0.12	Some small areas explained by shocks. $r$ based on [S II] $\lambda$ 6717,6731/H $\alpha$ . $r$ based on [O I] $\lambda$ 6300/H $\alpha$ not reliable.
ESO 297-G012	Young stars and shocks	-0.56	$r$ based on [N II] $\lambda$ 6584/H $\alpha$ . $r$ based on [O I] $\lambda$ 6300/H $\alpha$ or [S II] $\lambda$ 6717,6731/H $\alpha$ not reliable.
F06076–2139	...	0.75	$r$ based on [N II] $\lambda$ 6584/H $\alpha$ data. No [O I] $\lambda$ 6300 nor [S II] $\lambda$ 6717,6731 data.
F06259–4708 P1	Young stars	0.74	Low velocity (100-150 km s <sup>-1</sup> ) shocks also present.
F06259–4708 P2	Shocks (100-150 km s <sup>-1</sup> ) and young stars	0.31	
08424–3130	Stars and shocks (~ 100 km s <sup>-1</sup> )	0.61	$r$ based on [S II] $\lambda$ 6717,6731/H $\alpha$ . $r$ based on [O I] $\lambda$ 6300/H $\alpha$ not reliable. Northern galaxy mainly shocks; southern one mainly stars.
F08520–6850	Stars and shocks (~ 100 km s <sup>-1</sup> )	0.40	
IC563	Young stars	0.22	Low velocity (100-150 km s <sup>-1</sup> ) shocks could be also present.
IC564 N	Young stars	0.44	Low velocity (100-150 km s <sup>-1</sup> ) shocks also present. $r$ based on [N II] $\lambda$ 6584/H $\alpha$ . No [O I] $\lambda$ 6300 data. $r$ based on [S II] $\lambda$ 6717,6731/H $\alpha$ not reliable.
IC564 S	Young stars	0.34	$r$ based on [N II] $\lambda$ 6584/H $\alpha$ . No [O I] $\lambda$ 6300 data. $r$ based on [S II] $\lambda$ 6717,6731/H $\alpha$ not reliable.
12042–3140	Young stars and shocks (100-150 km s <sup>-1</sup> )	0.81	Northern galaxy mainly stars, Southern one shocks.
12596–1529	Young stars and low velocity shocks	0.47	$r$ based on [S II] $\lambda$ 6717,6731/H $\alpha$ data. No [O I] $\lambda$ 6300 data. $r$ based on [S II] $\lambda$ 6717,6731/H $\alpha$ not reliable.
F14544–4255 E	Young stars	0.67	$r$ based on [S II] $\lambda$ 6717,6731/H $\alpha$ . No [O I] $\lambda$ 6300 data.
F14544–4255 W <sup>(d)</sup>	High velocity (100-300 km s <sup>-1</sup> ) shocks	0.67	Shocks may be associated to the nucleus according to the [O I] $\lambda$ 6300/H $\alpha$ map.
18093–5744 N	Young stars	0.09	Low velocity shocks also possible.
18093–5744 C	Stars older than 3 Myr and/or with $Z < Z_{\odot}$	-0.65	$r$ based on [S II] $\lambda$ 6717,6731/H $\alpha$ . $r$ based on [O I] $\lambda$ 6300/H $\alpha$ not reliable.
18093–5744 S	Young stars	0.27	
Class 2			
F04315–0840	Shocks (100-200 km s <sup>-1</sup> ) and young stars	0.63	Young stars in the inner region and arms/tidal tails. Shocks at 2-3 kpc from the nucleus.
08355–4944	Young stars	0.14	Low velocity shocks also present at ~ 2 kpc from the nucleus.
F10038–3338	Shocks (100-200 km s <sup>-1</sup> )	0.50	Shocks may be associated to the nucleus.
10257–4338	Shocks (100-150 km s <sup>-1</sup> ) and stars	0.63	
12116–5615	Young stars and low velocity shocks	0.57	
13001–2339	Shocks (100-150 km s <sup>-1</sup> )	0.48	All data with [O I] $\lambda$ 6300/H $\alpha$ > -1.2. Part of the shocks may be associated to the nucleus
17138–1017	Young stars and low velocity shocks	-0.23	No [O I] $\lambda$ 6300 data; $r$ according to [S II] $\lambda$ 6717,6731/H $\alpha$ data
21453–3511 <sup>(d)</sup>	High velocity (100-300 km s <sup>-1</sup> ) shocks and/or AGN.	0.76	Young stars (spiral arms). Shocks may be associated to the nucleus according [O I] $\lambda$ 6300/H $\alpha$ map.

<sup>(a)</sup> At least otherwise indicated, based on the comparison of the data with several ionization models in the [O I] $\lambda$ 6300/H $\alpha$ - [N II] $\lambda$ 6584/H $\alpha$  diagnostic diagram. For the present analysis solar metallicity has been considered as baseline. If higher metallicity (e.g.  $Z=2Z_{\odot}$ ) is considered, a higher presence of shocks with respect to stars would have been obtained (see Figure 9).

<sup>(b)</sup> Pearson coefficient inferred from the [O I] $\lambda$ 6300/H $\alpha$ -  $\sigma$  relation (see text). For objects where [O I] $\lambda$ 6300 was not detected or the  $r$  coefficient did not reach a confidence level of 90%,  $r$  was obtained from the [S II] $\lambda$ 6717,6731/H $\alpha$  or [N II] $\lambda$ 6584/H $\alpha$ , as indicated.

<sup>(c)</sup> Classified as Seyfert (Kewley et al. 2001a).

<sup>(d)</sup> Classified as Seyfert (Corbett et al. 2003).

**Table 4.** Linear Pearson correlation coefficients  $r$  and 1-degree polynomial fits for the different morphological groups considered here.

Group	[N II] $\lambda$ 6584/H $\alpha$		[S II] $\lambda$ 6717,6731/H $\alpha$		[O I] $\lambda$ 6300/H $\alpha$	
	$r$	A+Bx	$r$	A+Bx	$r$	A+Bx
All	0.43	-1.08 + 0.44 x	0.33	-1.44 + 0.55 x	0.54	-3.12 + 1.02 x
Class 0	0.54	-1.17 + 0.54 x	0.23	-1.00 + 0.28 x	0.30	-2.95 + 0.88 x
Class 1	0.43	-1.23 + 0.50 x	0.33	-1.55 + 0.60 x	0.48	-3.14 + 1.01 x
Class 2	0.31	-0.79 + 0.27 x	0.60	-1.18 + 0.69 x	0.61	-3.00 + 0.97 x

**Table 5.** Linear Pearson correlation coefficients  $r$  and linear fits for for the class 1 and 2 LIRGs distributed in luminosity groups spanning the entire luminosity range.

Luminosity Range ( $\log(L/L_{\odot})$ )	[N II] $\lambda$ 6584/H $\alpha$		[S II] $\lambda$ 6717,6731/H $\alpha$		[O I] $\lambda$ 6300/H $\alpha$	
	$r$	A+Bx	$r$	A+Bx	$r$	A+Bx
11.00-11.25	0.49	-0.97 + 0.39 x	0.63	-1.39 + 0.54 x	-0.05	-1.12 - 0.09 x
11.25-11.50	0.72	-1.24 + 0.51 x	0.63	-1.19 + 0.37 x	0.68	-3.09 + 1.01 x
11.50-11.75	0.28	-0.77 + 0.22 x	0.24	-0.81 + 0.20 x	0.35	-2.47 + 0.61 x
11.75-12.00	0.59	-1.58 + 0.64 x	0.43	-1.21 + 0.41 x	0.46	-3.01 + 0.95 x

**Table 6.** Linear Pearson correlation coefficients  $r$  and linear fits for all C1 and C2 LIRGs and ULIRGs

Group	[N II] $\lambda$ 6584/H $\alpha$		[S II] $\lambda$ 6717,6731/H $\alpha$		[O I] $\lambda$ 6300/H $\alpha$	
	$r$	A+Bx	$r$	A+Bx	$r$	A+Bx
ULIRGs MAC06	0.61	-1.99 + 0.82 x	0.51	-1.36 + 0.50 x	0.71	-3.15 + 1.11 x
LIRGs C1+C2	0.38	-0.96 + 0.35 x	0.41	-1.09 + 0.36 x	0.45	-2.74 + 0.79 x

FULL VERSION at <http://www.damir.iem.csic.es/extragalactic/publications/publications.html>

**Fig. 14.** Panel showing the images utilized for the morphological classification. The left column contains details about the size and scale for the displayed images, as well as relevant morphological features and final classification. The central and right columns display the *Digital Sky Survey* and HST images, respectively. Orientation is north up, east to the left.

FULL VERSION at <http://www.damir.iem.csic.es/extragalactic/publications/publications.html>

Fig. 14. continued.

FULL VERSION at <http://www.damir.iem.csic.es/extragalactic/publications/publications.html>

Fig. 14. continued.

FULL VERSION at <http://www.damir.iem.csic.es/extragalactic/publications/publications.html>

Fig. 14. continued.

FULL VERSION at <http://www.damir.iem.csic.es/extragalactic/publications/publications.html>

Fig. 14. continued.

FULL VERSION at <http://www.damir.iem.csic.es/extragalactic/publications/publications.html>

Fig. 14. continued.

FULL VERSION at <http://www.damir.iem.csic.es/extragalactic/publications/publications.html>

Fig. 14. continued.

FULL VERSION at <http://www.damir.iem.csic.es/extragalactic/publications/publications.html>

**Fig. 15.**  $[S\text{ II}]\lambda\lambda 6717,6731/H\alpha$  vs.  $[N\text{ II}]\lambda 6584/H\alpha$  diagrams for the individual pointings.

FULL VERSION at <http://www.damir.iem.csic.es/extragalactic/publications/publications.html>

Fig. 15. continued.

FULL VERSION at <http://www.damir.iem.csic.es/extragalactic/publications/publications.html>

**Fig. 16.**  $[O\text{ I}]\lambda 6300/H\alpha$  vs.  $[N\text{ II}]\lambda 6584/H\alpha$  diagrams for the individual pointings.

FULL VERSION at <http://www.damir.iem.csic.es/extragalactic/publications/publications.html>

Fig. 16. continued.

FULL VERSION at <http://www.damir.iem.csic.es/extragalactic/publications/publications.html>

**Fig. 17.** Line ratios vs. velocity dispersions relation for the individual pointings.

FULL VERSION at <http://www.damir.iem.csic.es/extragalactic/publications/publications.html>

Fig. 17. continued.

FULL VERSION at <http://www.damir.iem.csic.es/extragalactic/publications/publications.html>

Fig. 17. continued.

FULL VERSION at <http://www.damir.iem.csic.es/extragalactic/publications/publications.html>

Fig. 17. continued.

FULL VERSION at <http://www.damir.iem.csic.es/extragalactic/publications/publications.html>

Fig. 17. continued.

FULL VERSION at <http://www.damir.iem.csic.es/extragalactic/publications/publications.html>

Fig. 17. continued.

FULL VERSION at <http://www.damir.iem.csic.es/extragalactic/publications/publications.html>

Fig. 17. continued.